

Bayesian Sparse Vector Autoregressive Switching Models with Application to Human Gesture Phase Segmentation

Beniamino Hadj-Amar¹, Jack Jewson², and Marina Vannucci¹

¹*Department of Statistics, Rice University, TX 77005-1827*

²*Department of Economics and Business, Universitat Pompeu Fabra, Barcelona, Spain, 08005
beniamino.hadj-amar@rice.edu, jack.jewson@upf.edu, marina@rice.edu*

March 2024

Abstract

We propose a sparse vector autoregressive (VAR) hidden semi-Markov model (HSMM) for modeling temporal and contemporaneous (e.g. spatial) dependencies in multivariate nonstationary time series. The HSMM's generic state distribution is embedded in a special transition matrix structure, facilitating efficient likelihood evaluations and arbitrary approximation accuracy. To promote sparsity of the VAR coefficients, we deploy an l_1 -ball projection prior, which combines differentiability with a positive probability of obtaining exact zeros, achieving variable selection within each switching state. This also facilitates posterior estimation via Hamiltonian Monte Carlo (HMC). We further place non-local priors on the parameters of the HSMM dwell distribution improving the ability of Bayesian model selection to distinguish whether the data is better supported by the simpler hidden Markov model (HMM), or the more flexible HSMM. Our proposed methodology is illustrated via an application to human gesture phase segmentation based on sensor data, where we successfully identify and characterize the periods of rest and active gesturing, as well as the dynamical patterns involved in the gesture movements associated with each of these states.

Keywords: Hidden Semi-Markov Models; Vector Autoregressive; Sparsity; Switching Models; Gesture Phase Segmentation;

1 Introduction

Vector autoregressive (VAR) models offer a principled methodology for detecting the dynamics and connections between multiple time-series (Sims, 1980; Lütkepohl, 2005), wherein the observed data is assumed to be a noisy linear combination of some finite set of past observations. VAR models have proven to be especially useful in applications to complex data, for example in the analysis of the dynamical behaviours of economic and financial time series (Watson, 1994; Ahelegbey et al., 2016; Kalli and Griffin, 2018), and of high-dimensional signals arising from different areas of the brain, such as fMRI (Goebel et al., 2003) and EEG data (Prado et al., 2006; Kammerdiner and Pardalos, 2010). Nonstationarity is commonly observed in many physiological time series, as a result of external perturbations or due to an individual performing distinct tasks or experiences (Ombao et al., 2018; Hadj-Amar et al., 2021). In the application of this paper, we consider multivariate time series data that arise from a study on human gesture phase segmentation based on sensor data. Phase segmentation aims at identifying and characterising the principal units, the underlying hidden states of interest to practitioners, and the dynamical patterns involved in the gesture movements associated with each of these states (Moni and Ali, 2009; Wagner et al., 2014). Here, we analyse scalar velocity and acceleration recordings collected at discrete time intervals on the left hand, right hand, left wrist, and right wrist of an individual who is asked to read two distinct comic strips and to tell the stories in front of a sensor (Madeo et al., 2013). As a segmentation exercise, we aim to model the data to identify, in an automated fashion, the periods of rest and active gesturing. Automating such a classification circumvents a human being from conducting such a laborious, time consuming and ultimately expensive task and allowing linguists greater resources to investigate the interaction between speech, gestures and discourse.

There are two main tasks when analysing this data, which motivated the methodological development of our proposed model. The first is to *classify* whether a particular gesture phase corresponds to a resting or active state. While Sarkar et al. (2023) considered several supervised machine learning methods for this task, Wagner et al. (2014) reported ambiguity in the problem of analysing gestures and serious disagreement, even among experts, in determining when a gesture unit starts and ends. It is, therefore, of interest whether unsupervised, hidden state models can replicate supervised classification labels and help address these differences of opinion in a data driven fashion. A second main task of the analysis is to *investigate the dynamic associations* of acceleration and velocity measurements collected from left hand (LF), right hand (RH), left wrist (LW), and right wrist (RW) and how they

differ between resting and active states. We combine several recent individual works to achieve these goals. In particular, our unified approach considers: (i) hidden state models with VAR emissions and general dwell distributions; (ii) non-local priors for improved selection between nested dwell distributions; (iii) the l_1 -ball projection prior for model selection and estimation of the VAR parameters.

VAR Hidden Markov Models (VAR HMM), also called VAR Markov switching processes (Hamilton, 1989; Fox et al., 2014; Samdin et al., 2016), have proven useful in modeling nonstationary streams of data. Formally, a VAR-HMM is a stochastic process which is based on an unobserved (hidden) state sequence that takes discrete values and whose transition probabilities follow a Markovian structure. Conditioned on the state sequence, the observations are assumed to be generated from a state-specific VAR process. Although computationally convenient, assuming that the hidden states are Markovian limits the flexibility of HMMs. In particular, the dwell duration in any state, namely the number of consecutive time points that the time series spends in that state, implicitly follows a geometric distribution, an assumption that has been shown to be unrealistic in many data applications (Zen et al., 2007; Pimentel et al., 2015; Hadj-Amar et al., 2023). Hidden semi-Markov Models (HSMMs) provide a more general framework by introducing an explicit, state specific, form for the dwell duration (Guédon, 2003). We consider for the first time HSMM models with VAR emission distributions and facilitate Bayesian inference (Hadj-Amar et al., 2023) via the likelihood approximation introduced by Langrock and Zucchini (2011), in which a special structure of the transition matrix is used to model the state duration distributions. This allows us to select, in a data driven manner, which dwell distribution is best supported by the data and therefore leads to improved state classification.

To expedite this selection, we place non-local priors (Johnson and Rossell, 2012) on the parameters of the HSMM dwell distribution, improving the ability of Bayesian model selection to distinguish whether the data is better supported by the simpler HMM, or a more flexible HSMM. While non-local priors have been previously deployed for linear regression (Rossell and Telesca, 2017) and Gaussian mixture modelling (Fúquene et al., 2019) we extend this to more general nested model selection problems.

Capturing the complex multivariate dependencies in human gesture data applications requires modelling not only the serial dependence within each univariate series, but also the interdependence across distinct physiological measurements, both within and across time points. To achieve this, we consider VAR HSMM models that allow temporal and contemporaneous (e.g. spatial) dependencies

in the non-stationary time series (Paci and Consonni, 2020; Hadj-Amar et al., 2023). VAR models are generally overparametrised, allowing for dependence between all dimensions of the multivariate time series where the true dependence structure is often much sparser. Shrinkage priors, such as the Minnesota prior (Doan et al., 1984) and numerous variations (Kadiyala and Karlsson, 1997; Lütkepohl, 2005), the doubly adaptive elastic-net LASSO (Gefang, 2014), and the Bayesian nonparametric LASSO (Billio et al., 2019) have been used for VAR coefficients, but, often arbitrary, post-hoc thresholding is required to estimate the zeros. A common framework to introduce exact zeros into a Bayesian analysis is to use spike-and-slab priors (George and McCulloch, 1993; Chiang et al., 2017). Here, we deploy, for the first time, the novel l_1 -ball projection prior (Xu and Duan, 2023), a prior with mass at exact zeros, on the coefficients of the VAR matrices. Such a prior introduces unconstrained latent variables and transforms them onto the space of VAR parameters in a way that provides positive probability that any element is exactly zero. Importantly, the transformation is almost surely continuous and differentiable, allowing us to estimate edge inclusion probabilities while remaining compatible with efficient posterior sampling using algorithms such as Hamiltonian Monte Carlo (HMC, Duane et al. 1987) and off-the-shelf probabilistic programming languages such as *stan* (Carpenter et al., 2016). Lastly, we place standard priors on the state specific covariance matrices that capture contemporaneous spatial dependencies, taking advantage of *stan* implementations that use the Cholesky decomposition.

We show on simulated data how our model is able to detect sparse VAR structure across hidden switching regimes as well as estimate contemporaneous dependencies and conduct model selection between the simpler HMM and the more flexible HSMM model. Applied to the gesture phase data, unsupervised learning appears to perform well for resting and active state classification, showing potential to address some of the ‘disagreements between experts’ and dwell times in these states appear better modelled by a negative binomial distribution than a geometric distribution, achieving better model fit and state classification. Further, our model also estimated interpretable VAR structures with differing levels of sparsity across the states and successfully characterises and predicts a new video, corresponding to a different, unseen, story.

The rest of the paper is organised as follows: Section 2 introduces our VAR HSMM model, the l_1 -ball prior utilized to impose sparsity on the temporal connections and our strategy for posterior inference. Section 3 contains our simulation study, including comparisons of the selection performance of local and non-local priors. Lastly, Section 4 presents our application to the gesture phase data and Section 5 concludes the paper with a discussion. The *stan* files (and R utilities) that were used to

implement our analysis are available at <https://github.com/Beniamino92/sparseVARHSMM>. We use the probabilistic programming framework associated with *stan*, which facilitates extensions of the code to similar applications.

2 VAR Approximate HSMMs

We describe our proposed vector autoregressive (VAR) hidden semi-Markov model (HSMM) for modelling temporal and contemporaneous (e.g. spatial) dependencies in high-dimensional nonstationary time series.

2.1 Vector Autoregressive Emissions

Let $\mathbf{y} = \{\mathbf{y}_t\}_{t=1}^T$ be D dimensional observed time series, with $\mathbf{y}_t = (y_{t1}, \dots, y_{tD}) \in \mathbb{R}^D$, and let $\mathbf{z} = (z_1, \dots, z_T)$ indicate the hidden states associated with each time point, with $z_t \in \{1, \dots, K\}$ and $K \in \mathbb{Z}_+$ the number of latent states. Conditional on the value of the hidden state sequence z_t , the data \mathbf{y}_t are modelled through a state-specific VAR process of order $P \in \mathbb{Z}_+$, which assumes \mathbf{y}_t to be a linear combination of past observations $\mathbf{y}_{t-1:t-P}$, across all dimensions, plus a Gaussian noise term, as

$$\mathbf{y}_t | z_t = j \sim \mathcal{N}_D \left(\boldsymbol{\alpha}^j + \sum_{p=1}^P \boldsymbol{\Theta}_p^j \mathbf{y}_{t-p}, \boldsymbol{\Sigma}^j \right), \quad t = P+1, \dots, T, \quad (2.1)$$

where for each regime $j = 1, \dots, K$, $\boldsymbol{\alpha}^j \in \mathbb{R}^D$ is a vector of state-dependent intercepts, that allow for the possibility of a non-zero mean $\mathbb{E}[\mathbf{y}_t | \mathbf{y}_{t-1:t-P}]$, and $\boldsymbol{\Theta}_p^j = \{\theta_{pil}^j\}_{i,l=1}^D \in \mathbb{R}^{D \times D}$ is the matrix of autoregressive coefficients at lag $p = 1, \dots, P$.

Unlike common approaches that assume independent noise across dimensions, for computational convenience, (2.1) allows for contemporaneous dependencies as well as temporal dependencies via a state specific positive definite covariance matrix $\boldsymbol{\Sigma}^j = \{\sigma_{il}^j\}$. We decompose $\boldsymbol{\Sigma}^j$ into a vector of scales $\boldsymbol{\tau}^j$ and a correlation matrix $\boldsymbol{\Omega}^j = \{\omega_{il}^j\}$, where $\tau_i^j = \sqrt{\sigma_{ii}^j}$ and $\omega_{il}^j = \frac{\sigma_{il}^j}{\tau_i^j \tau_l^j}$ (Gelman and Hill, 2006). Given standardised data, we set $\tau_i^j \sim \text{Cauchy}(0.5, 0.5) \mathbb{I}(\tau_i^j > 0)$, providing high prior probability of relatively small scales but with heavy tails to ensure that the prior does not overly regularise a regime with greater variance. Then, we specify the prior for the correlation matrices as

$$\boldsymbol{\Omega}^j \sim \text{LKJ}(\boldsymbol{\Omega}^j; \xi) \propto \det(\boldsymbol{\Omega}^j)^{\xi-1},$$

where LKJ denotes the prior proposed by (Lewandowski et al., 2009), namely a family of probability distribution for positive definite correlation matrices (or equivalently for their Cholesky factors). Setting $\xi = 1$ provides a uniform distribution over correlation matrices. Note this is different from a uniform distribution over elements of the correlation matrix, as $\mathbf{\Omega}^j$ is constrained to be symmetric and positive definite. Such a choice of prior allows us to input no prior information about the strength of contemporaneous dependencies, while ensuring that the covariance matrix is positive definite. This prior implemented in *stan* via the Cholesky decomposition (Stan Development Team, 2018).

2.2 Introducing Sparsity in the VAR Coefficients via the l_1 -ball Projection Prior

Shrinkage priors are commonly used (Doan et al., 1984; Gefang, 2014; Billio et al., 2019) to deal with over parametrisation in VAR models. The number of distinct elements of $\Theta = \{\Theta^j\}_{j=1}^K$, with $\Theta^j := \{\Theta_p^j\}_{p=1}^P$, for $j = 1, \dots, K$, is KPD^2 , which grows quickly even for moderate dimensional data. Here, we deploy the recently proposed l_1 -ball projection prior of Xu and Duan (2023), which augments the sample space with strictly continuous latent parameters and applies an almost surely continuous and differentiable transformation that results in model parameters with a mixture-type prior including positive probability of exact 0’s and continuous density away from 0. Continuity and differentiability of the l_1 -ball projection prior allows for efficient posterior sampling using algorithms such as Hamiltonian Monte Carlo (HMC, Duane et al. 1987). Xu and Duan (2023) note that the classic spike-and-slab prior can be viewed as a special case of the l_1 -ball prior and demonstrate empirically that the l_1 -ball prior leads to faster mixing performance than discrete spike-and-slab.

Before formally defining the l_1 -ball projection prior we provide an intuitive illustration. We introduce unconstrained latent variables, β^j , and transform them onto the space of VAR parameters, θ^j , in a way that provides positive probability that any element is exactly zero. The degree of sparsity in the transformation is controlled by a positive scalar-valued random variable called the radius r^j . Figure 1 displays the l_1 -ball projection in \mathbb{R}^2 with $r^j = 2$. Any β^j values in the dotted ‘V’s away from the axis have one of their coordinates mapped to 0 in θ^j , e.g. the two red lines at $\beta^j = (-10, 2)$ and $\beta^j = (-7, -3)$ which are both mapped to $\theta^j = (-r^j, 0)$. Alternatively, for β^j values in the diagonal columns going away from the origin, neither coordinate is mapped to 0 in θ^j , e.g. the blue point $\beta^j = (3, 4.2)$ is mapped to $\theta^j = (0.4, 1.6)$, and both $\beta^j = (5.5, 4.5)$ and $\beta^j = (9.5, 8.5)$ are mapped to $\theta^j = (1.5, 0.5)$.

Formally, define $\beta_p^j = (\beta_{p1}^j, \dots, \beta_{pD^2}^j) = \text{vec}(\mathbf{B}_p^j)$, with each element of matrix $\mathbf{B}_p^j = \{\beta_{pil}^j\}_{i,l=1}^D \in$

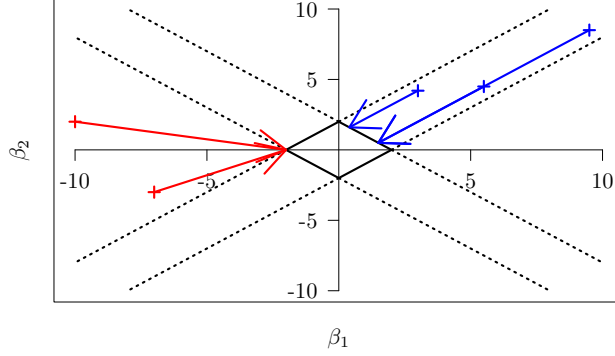


Figure 1: l_1 -ball projection in \mathbb{R}^2 mapping β^j to θ^j with radius $r^j = 2$. Any β^j 's in the dotted 'V's away from the axis has one of their coordinates mapped to 0 in θ^j , while any β^j 's in the diagonal columns going away from the origin do not have either coordinate mapped to 0.

$\mathbb{R}^{D \times D}$ corresponding to the latent parameter associated with each autoregressive coefficient. Similarly, we define $\theta_p^j = (\theta_{p1}^j, \dots, \theta_{pD^2}^j) = \text{vec}(\Theta_p^j)$. Here, the $\text{vec}(\cdot)$ operator denotes the vectorization of a matrix into a column vector, i.e. $\text{vec} : \mathbb{R}^{D \times D} \rightarrow \mathbb{R}^{D^2}$. Further, we construct the vector of state-specific latent parameters $\beta^j = [\beta_1^j, \dots, \beta_P^j]'$ and autoregressive parameters $\theta^j = [\theta_1^j, \dots, \theta_P^j]'$, by concatenating the corresponding vector of lag-specific elements. Then, the l_1 -ball projection can be specified as

$$\{\beta_{pil}^j\}_{i,l=1}^D \stackrel{\text{iid}}{\sim} \text{DExp}(0, \sigma_\beta^j), \quad r^j \stackrel{\text{iid}}{\sim} \text{Expo}(a_r^j) \quad (2.2)$$

$$\theta^j := \arg \min_{\|\mathbf{x}\|_1 \leq r^j} \|\beta^j - \mathbf{x}\|_2^2, \quad \Theta_p^j := \text{vec}^{-1}(\theta_p^j), \quad \text{for } p = 1, \dots, P, \quad (2.3)$$

for $j = 1, \dots, K$, where $\|\cdot\|_1$ and $\|\cdot\|_2$ denote the l_1 and l_2 norms, respectively, and where the state-specific radius is $r^j > 0$. The operator $\text{vec}(\cdot)^{-1}$ represents the inverse of the vectorization operator, i.e. $\text{vec}^{-1} : \mathbb{R}^{D^2} \rightarrow \mathbb{R}^{D \times D}$ such that $\text{vec}(\text{vec}^{-1}(\theta_p^j)) = \theta_p^j$, $\text{Expo}(a)$ represents an exponential distribution with rate a , and $\text{DExp}(\mu_\beta, \sigma_\beta)$ represents a double-exponential (often called a Laplace distribution) with mean μ_β and scale parameter σ_β .

We employ the l_1 -ball projection prior construction (2.2)-(2.3) independently in each regime: a double exponential distribution is assumed on random variables β_{pil}^j ; the l_1 -ball projection with radius r^j is applied to map $\beta^j \mapsto \theta^j$ such that if $\|\beta^j\|_1 \geq r^j$ then $\|\theta^j\|_1 = r^j$ with some of the $\theta_{pil}^j = 0$; the matrix of autoregressive coefficients Θ_p^j is reconstructed using the vec^{-1} operator. The loss function in Eq. (2.3) is strictly convex, namely for every β^j , there is only one optimal solution θ^j . The projection can be solved using a variant of the procedure by [Duchi et al. \(2008\)](#) and [Xu and Duan](#)

(2023), which is summarized in Algorithm A.1 in the Supplementary Material. This mapping function is almost surely continuous and differentiable, its Jacobian is equal to one, invariant to the number of non-zero elements.

2.3 Switching Model with Arbitrary Dwell Distribution

Popular hidden state models assume that the latent state sequence \mathbf{z} evolves as a Markov process and corresponds to assuming the dwell time in each state is geometrically distributed. However, there is no reason beyond computational convenience to believe that dwell times in active and resting states are geometric. We instead model the hidden states \mathbf{z} as evolving according to a hidden semi-Markov model (HSMM) with general dwell duration distributions $\{p(d_j = s | \boldsymbol{\lambda}^j)\}_{j=1}^K$ parametrised by $\{\boldsymbol{\lambda}^j\}_{j=1}^K$ (e.g. the rate and dispersion of a negative binomial distribution). This generalised framework allows us to consider several possible dwell distributions (including the HMM) and see which is best supported by the data. Following Langrock and Zucchini (2011) and Hadj-Amar et al. (2023), such a HSMM can be approximated by an extended state-space HMM with latent states $\mathbf{z}^* = (z_1^*, \dots, z_T^*) \in \{1, 2, \dots, \bar{B}\}$, where $\bar{B} = \sum_{i=1}^K b_i$ and $\mathbf{b} = (b_1, \dots, b_K)$ are fixed positive integers (*thresholds*). Each HSMM state is mapped to a group of b_j HMM states that are associated with the same VAR emission distribution (Eq. 2.1), and these group of states is called a *state aggregate* $B_j = \{\bar{b} : \sum_{i=0}^{j-1} b_i < \bar{b} \leq \sum_{i=0}^j b_i, b_0 = 0\}$. The HSMM dwell time d_j then correspond to the number of consecutive time points that the latent state is a member of the state aggregate B_j . The state aggregates allow the HMM to capture the more complex HSMM dwell distributions through the special structure of the Markov state transition matrix $\mathbf{A} = \{A_{il}\}_{i,l=1}^{\bar{B}}$, where $A_{il} = p(z_t^* = l | z_{t-1}^* = i)$ are completely determined by the HSMM dwell distribution $p(d_j = s | \boldsymbol{\lambda}^j)$ (within state aggregate moves) and the between state aggregate transition probabilities $\boldsymbol{\pi}^j = (\pi_{j1}, \dots, \pi_{jK})$, in which $\pi_{jk} = p(z_t = k | z_{t-1} = j, z_t \neq j)$ for $j, k = 1, \dots, K$. Note that $\pi_{jj} = 0$, since self transitions are prohibited. See Supplementary Material for the exact form of the matrix \mathbf{A} .

The generative framework modelling the evolution dynamics of the hidden states can then be summarized as

$$\boldsymbol{\pi}^j \sim \text{Dirichlet}_{K-1}(\boldsymbol{\alpha}_0), \quad d_j \sim g(\boldsymbol{\lambda}^j), \quad \boldsymbol{\lambda}^j \sim G, \quad j = 1, \dots, K \quad (2.4)$$

$$z_t^* | z_{t-1}^* \sim \mathbf{A}_{z_{t-1}^*} \quad t = 1, \dots, T \quad \mathbf{A}_i := \psi(\boldsymbol{\pi}, \boldsymbol{\lambda}), \quad i = 1, \dots, \bar{B},$$

where, we assume that the initial state has distribution $\mathbf{A}_0 = (A_{01}, \dots, A_{0\bar{B}})$, e.g. $z_0^* \sim \mathbf{A}_0$, where

we follow a common practice and assume a uniform distribution for the initial state (Zucchini et al., 2017). Here $\psi(\cdot)$ indicate the mapping from $\boldsymbol{\pi} = \{\boldsymbol{\pi}^j\}_{j=1}^K$ and $\boldsymbol{\lambda} = \{\boldsymbol{\lambda}^j\}_{j=1}^K$ to the matrix \mathbf{A} , and \mathbf{A}_i denotes the i^{th} row of \mathbf{A} . Langrock and Zucchini (2011) showed that this formulation allows for the representation of any duration distribution, and yields an HMM that is, at least approximately, a reformulation of the underlying HSMM. Hadj-Amar et al. (2023) deployed a likelihood approximation method and showed that such a formulation can speed HSMM inference up considerably while incurring minimal statistical error.

To provide intuition about the extended state-space HMM, Figure 2 illustrates an example of formulating an HSMM through an HMM, where for the sake of the illustration, this representation is made exact, namely there is no approximation. A two-state HSMM characterized by emission distributions $f(\boldsymbol{\theta}_j)$, and dwell-duration distributions $d_j(r)$, for $j = 1, 2$, is represented as an HMM with extended state space $\bar{B} = 7$ with dwell-threshold $\mathbf{b} = (4, 3)$ for state aggregates B_1 and B_2 , respectively. Note that the dwell-thresholds are selected to cover the entire support of the duration distributions, so that this HMM formulation corresponds to its exact HSMM representation. The transition matrix \mathbf{A} is completely determined by the HSMM dwell distribution $p(d_j = r)$ (within state aggregate moves) and the between state aggregate transition probabilities π_{12} and π_{21} , which in this case are equal to one, since we consider a two-state HSMM.

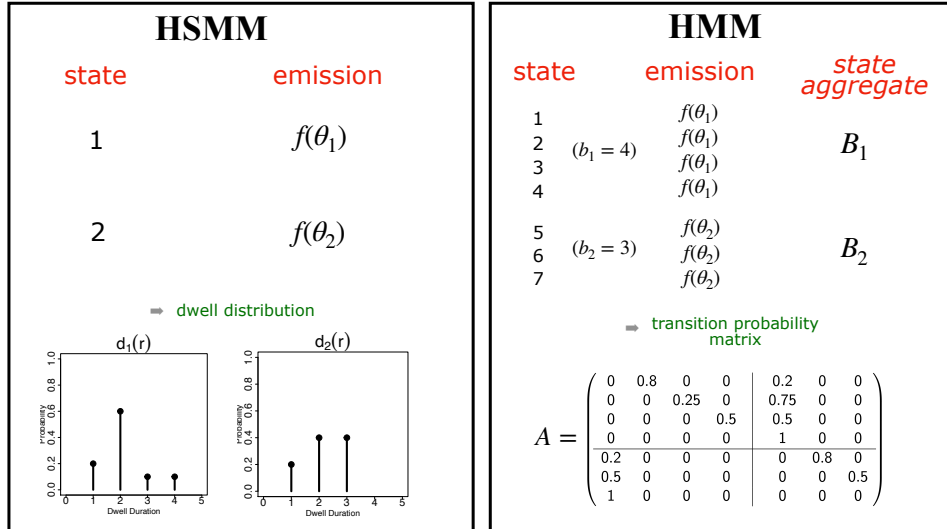


Figure 2: Example of formulating an HSMM through an HMM.

2.3.1 State-dwell parameters and non-local priors

Next, we specify the priors for the state dwell parameters λ^j . We consider two choices: the negative binomial distribution, and the geometric distribution (corresponding to the HMM). The negative binomial dwell distribution is parameterized by its mean and overdispersion parameter as $\lambda^j = \{m^j, \rho^j\}$ and constitutes a parsimonious extension of the geometric distribution, with the ability to capture over and under dispersion with only one extra parameter. The probability mass function of a negative-binomial, shifted to have strictly positive support, is given by

$$g^{NB}(d_j; \lambda^j) = \frac{\Gamma(d_j - 1 + \rho^j)}{\Gamma(\rho^j)(d_j - 1)} \left(\frac{\rho^j}{\rho^j + m^j} \right) \left(\frac{m^j}{\rho^j + \lambda^j} \right)^{d_j - 1}, \quad d_j = 1, 2, \dots \quad (2.5)$$

The mean dwell time under negative binomial dwell is $m^j + 1$ and its variance is $m^j + \frac{m^{j2}}{\rho^j}$. Note that the geometric distribution can be obtained from the negative binomial distribution for $\rho^j = 1$ and $m^j = \frac{\tilde{\pi}_{jj}}{1 - \tilde{\pi}_{jj}}$, where $\tilde{\pi}_{jj} := p(z_t = j | z_{t-1} = j)$ denotes the (Markovian) probability of self transitions in the HMM. Thus, for the negative binomial overdispersion parameters ρ^j , we consider two candidate priors: (i) a so called ‘local’-prior (LP), i.e. $p^{LP}(\rho^j) = \mathcal{IG}(\rho^j; c_0^{NB}, c_0^{NB} + 1)$ such that the prior mode at $\rho^j = 1$, namely the value of ρ^j that recovers the simpler HMM; (ii) a ‘non-local’ prior (NLP) (Johnson and Rossell, 2012) that assigns 0 density in the region around $\rho^j = 1$. Specifically, we place an exponential moment prior (*eMOM*) (Rossell and Telesca, 2017) prior on $\log \rho^j$,

$$p^{NLP}(\log \rho^j | \tau^j) = \exp \left\{ \sqrt{2} - \frac{v^j}{(\log \rho^j)^2} \right\} \times \mathcal{N}(\log \rho^j; 0, \sqrt{v^j}), \quad (2.6)$$

that has 0 density at $\log \rho^j = 0$. Compared with other NLP’s, the *eMOM* prior has lighter tails allowing for a prior that is non-local but still places high density on reasonable values. Figure 3 plots the *eMOM* prior for $\log \rho^j$ for several values of the hyperparameter v^j alongside the implied prior for ρ^j . For the mean parameter m^j , we specify a Gamma prior, namely $m^j \sim \mathcal{G}(a_0^{NB}, b_0^{NB})$.

The geometric dwell distribution is parameterized by the HMM state’s probabilities of self transition $\lambda^j = \{\tilde{\pi}_{jj}\}_{j=1}^K$, with probability mass function, shifted to have strictly positive support, given by

$$g^{geom}(d_j; \lambda^j) = (\tilde{\pi}_{jj})^{d_j - 1} (1 - \tilde{\pi}_{jj}), \quad d_j = 1, 2, \dots, \quad (2.7)$$

with mean dwell time specified as $\frac{1}{1 - \tilde{\pi}_{jj}}$. In this case, the HMM transition probabilities $\tilde{\pi}^j = (\tilde{\pi}_{j1}, \dots, \tilde{\pi}_{jK})$ are assigned a Dirichlet prior on the $(K-1)$ dimensional simplex, i.e. $\tilde{\pi}^j \sim \text{Dirichlet}_K(\delta_0^{Geom})$, for $j = 1, \dots, K$.

Figure 4 provides a graphical model depicting the structure of the proposed sparse VAR HSMM.

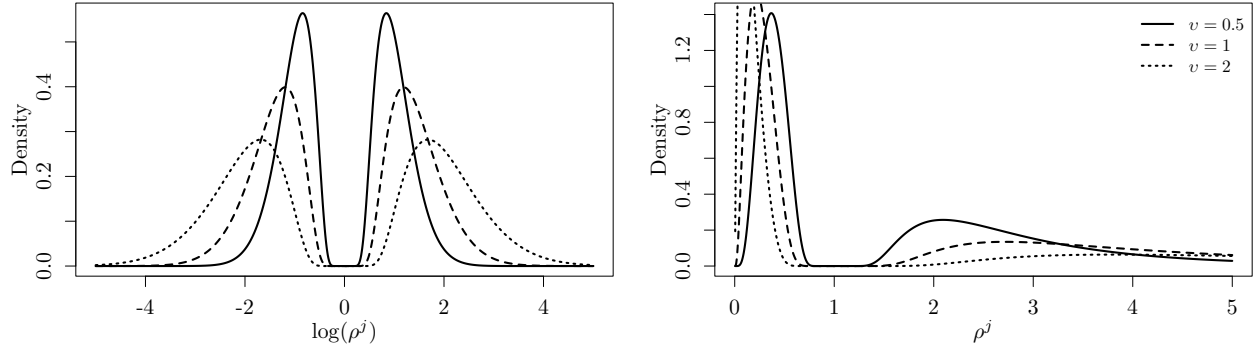


Figure 3: *The eMOM non-local prior for $\log \rho^j$ and the implied prior on ρ^j for several different values of the hyperparameter v^j .*

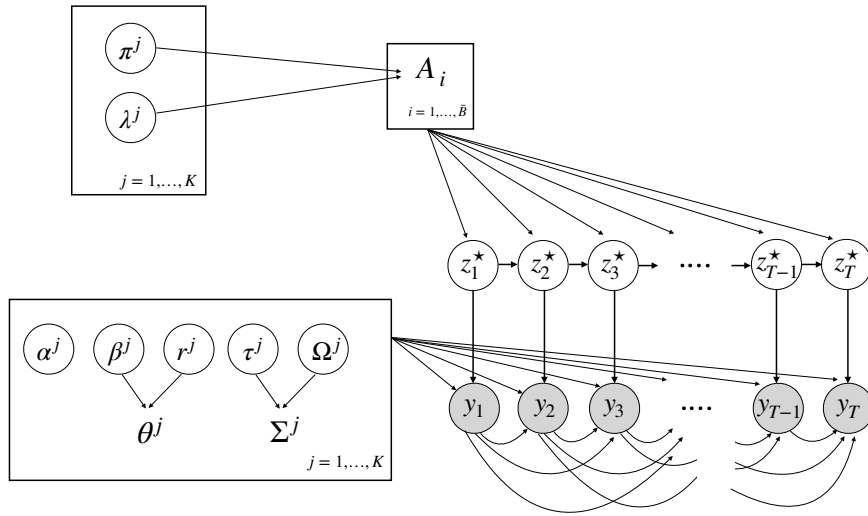


Figure 4: Graphical model representation of the proposed sparse VAR approximate HSMMs. Transition probabilities \mathbf{A}_i are solely determined by π_j and $g(\lambda_j)$, and thus the probabilities \mathbf{A}_i are not considered as random variables themselves. Similarly, while the likelihood depends on Θ^j and Σ^j , it is convenient to specify priors for latent parameters β^j , r^j , τ^j and Ω^j for reasons outlined in Sections 2.1 and 2.2.

2.4 Posterior Sampling

Let $\boldsymbol{\eta} = \{(\boldsymbol{\pi}^j, \boldsymbol{\lambda}^j, \boldsymbol{\alpha}^j, \boldsymbol{\beta}^j, r^j, \boldsymbol{\Omega}^j, \boldsymbol{\tau}^j)\}_{j=1}^K$ be the parameters of interest, where we recall that the autoregressive matrices $\boldsymbol{\Theta}^j$ are a deterministic transformation of parameters $\boldsymbol{\beta}^j$ and r^j through the l_1 -ball projection prior, and the covariance matrices $\boldsymbol{\Sigma}^j$ are constructed deterministically from $\boldsymbol{\Omega}^j$ and $\boldsymbol{\tau}^j$. Throughout, we denote prior distributions by $p(\cdot)$ and differentiate these from their corresponding posterior distributions $p(\cdot | y)$ by the conditioning on y . We write the posterior distribution as

$$p(\boldsymbol{\eta} | \mathbf{y}) \propto \mathcal{L}(\mathbf{y} | \boldsymbol{\eta}) \times \left[\prod_{j=1}^K p(\boldsymbol{\pi}^j) \times p(\boldsymbol{\lambda}^j) \times p(\boldsymbol{\alpha}^j) \times p(\boldsymbol{\beta}^j) \times p(r^j) \times p(\boldsymbol{\Omega}^j) \times p(\boldsymbol{\tau}^j) \right], \quad (2.8)$$

where the likelihood $\mathcal{L}(\cdot)$ is defined as

$$\mathcal{L}(\mathbf{y} | \boldsymbol{\eta}) = \boldsymbol{\pi}_0^{\star'} \mathbf{P}(\mathbf{y}_1) \mathbf{A} \mathbf{P}(\mathbf{y}_2) \mathbf{A} \cdots \mathbf{A} \mathbf{P}(\mathbf{y}_{T-1}) \mathbf{A} \mathbf{P}(\mathbf{y}_T) \mathbf{1}, \quad (2.9)$$

with the diagonal matrix $\mathbf{P}(y)$ of dimension $\bar{B} \times \bar{B}$ defined as

$$\mathbf{P}(\mathbf{y}) = \text{diag} \left\{ \underbrace{p(\mathbf{y} | \boldsymbol{\alpha}^1, \boldsymbol{\Theta}^1, \boldsymbol{\Sigma}^1), \dots, p(\mathbf{y} | \boldsymbol{\alpha}^1, \boldsymbol{\Theta}^1, \boldsymbol{\Sigma}^1)}_{b_1 \text{ times}}, \dots, \underbrace{p(\mathbf{y} | \boldsymbol{\alpha}^K, \boldsymbol{\Theta}^K, \boldsymbol{\Sigma}^K) \dots p(\mathbf{y} | \boldsymbol{\alpha}^K, \boldsymbol{\Theta}^K, \boldsymbol{\Sigma}^K)}_{b_K \text{ times}} \right\},$$

and $p(\mathbf{y} | \boldsymbol{\alpha}^j, \boldsymbol{\Theta}^j, \boldsymbol{\Sigma}^j)$ the probability density of the VAR emission distributions (Eq. 2.1). Here, $\mathbf{1}$ denotes an \bar{B} -dimensional column vector with all entries equal to one and $\boldsymbol{\pi}_0^{\star}$ represents the initial distribution for the state aggregates. Note that if we assume that the underlying Markov chain is stationary, $\boldsymbol{\pi}_0^{\star}$ is solely determined by the transition probabilities $\boldsymbol{\Phi}$, i.e. $\boldsymbol{\pi}_0^{\star} = (\mathbf{I} - \boldsymbol{\Phi} + \mathbf{U})^{-1} \mathbf{1}$, where \mathbf{I} is the identity matrix and \mathbf{U} is a square matrix of ones. Alternatively, it is possible to start from a specified state, namely assuming that $\boldsymbol{\pi}_0^{\star}$ is an appropriate unit vector, e.g. $(1, 0, \dots, 0)$, as suggested by [Leroux and Puterman \(1992\)](#). The computation of the likelihood in Eq. (2.9) is often subject to numerical underflow and hence its practical implementation usually requires appropriate scaling ([Zucchini et al., 2017](#)). Furthermore, for multivariate likelihoods the matrix multiplications are implemented on the log-scale.

The posterior distribution (2.8) is not available in closed form, therefore we conduct inference using MCMC methods. In particular, we use Hamiltonian Monte Carlo (HMC, [Duane et al. 1987](#)), which uses a discretisation of the Hamiltonian dynamics to propose a joint parameter update and accepts or rejects this with the usual Metropolis Hasting probability, and the No-U-Turn Sampler (NUTS) ([Hoffman and Gelman, 2014](#)), which automatically tunes the Hamiltonian step size to the geometry of

the targeted posterior. The combination of the two allows for efficient exploration of the multivariate parameter space. We take advantage of HMC and NUTS implementations available in the probabilistic programming language *stan* (Carpenter et al., 2016). All *stan* requires is that the user write out their model and the computations required to evaluate the likelihood and *stan* compiles the models and optimises sampling to its geometry.

The MCMC implementation outputs N samples $\{\boldsymbol{\eta}^{(i)}\}$, for $i = 1, \dots, N$, approximating the posterior distribution. These samples can be used to estimate posterior summaries such as means and variances for different parameters. A particular feature of the l_1 -ball prior is that posterior samples for any of the θ_{pil}^j , transformed from the corresponding samples of β_{pil}^j , may contain exact zeros. Therefore, the posterior probability for the presence of a temporal VAR connection between i and l in lag p and regime j is straightforward to estimate as the frequency of these samples that are non-zero. We further remark that the parameters θ_{pil}^j enter into the likelihood as a deterministic transformation of the parameters β_{pil}^j and r^j , which are easy to sample via HMC as they are strictly continuous. Further, *stan*'s compatibility with bridge sampling (Meng and Wong, 1996; Meng and Schilling, 2002; Gronau et al., 2020) allows for the use of posterior samples to estimate the marginal likelihood $p(\mathbf{y}) := \int \mathcal{L}(\mathbf{y} | \boldsymbol{\eta}) p(\boldsymbol{\eta}) d\boldsymbol{\eta}$ and conduct Bayesian model selection for the dwell distribution as in Hadj-Amar et al. (2023). Similarly to Hadj-Amar et al. (2023), our implementation is able to take advantage of the sparse nature of the state transition matrix \mathbf{A} to provide considerable speed up. Section A.2 details some reparametrizations that were used to improve mixing.

3 Simulation Studies

3.1 Data generation

To investigate the performance of our model we simulated a $D = 5$ -dimensional time series consisting of $T = 400$ observations from a $K = 3$ state HSMM with VAR emission distributions of order $P = 2$ in each regime. The dwell times in each state j were generated from negative binomial distributions $NB(\lambda_j, \rho_j)$ with mean parameters $\lambda_1 = 2$, $\lambda_2 = 10$ and $\lambda_3 = 7$ and overdispersion parameters $\rho_1 = 0.25$, $\rho_2 = 3$ and $\rho_3 = 5$. The between state transition probabilities π_{jk} were set to 0.5, for $j \neq k = 1, 2, 3$. The VAR parameters were generated such that state 1 was 70% sparse, state 2 was 30% sparse and state 3 was 90% sparse. Non-zero elements of each Θ_p^j were generated such that they were positive or negative with equal probability and their absolute value was sampled uniformly between 0.2 and 0.8.

Additionally, a rejection step was done to check that the sampled values constituted a stable VAR process. State specific intercept values α^j were sampled uniformly between -4 and 4. Finally, the covariance matrices Σ^j were generated as $\Sigma = \mathbf{P}' \text{diag}(\sigma_1, \dots, \sigma_D) \mathbf{P}$, with \mathbf{P} being an orthogonal matrix and σ_i assumed positive. The matrix \mathbf{P} was constructed by orthogonalizing a random matrix whose entries were simulated from a standard Normal, while each σ_i was uniformly sampled in the interval $[1, 3]$. The data were standardised such that the time series in each dimension had mean 0 and variance 1. The top plot of Figure 5 shows all dimensions of the time series and the true state sequence.

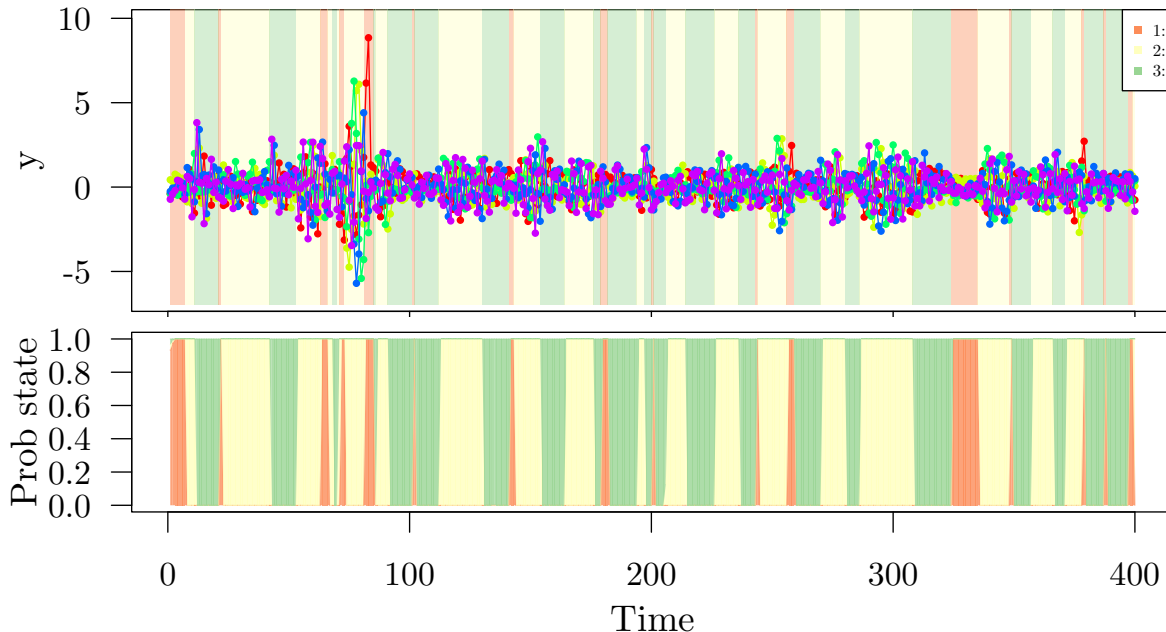


Figure 5: Simulation Study. Simulated $D = 5$ dimensional time series, plotted on top of one-another, along with the hidden states (top) and state probabilities estimated by the HSMM- l_1 -NLP (bottom).

3.2 Parameter settings

To facilitate Bayesian model selection between the HMM and HSMM, [Hadj-Amar et al. \(2023\)](#) proposed setting HSMM prior hyperparameters a_0^{NB} and b_0^{NB} to match the prior mean and variance of the expected dwell time to that of an HMM with Dirichlet priors on its transition matrix. We elicited the prior mean expected dwell to be 10 with standard deviation 5, providing an uninformative prior and

considerable mass away from very short dwell times. Parameters δ_0^{Geom} and δ_0^{NB} can be elicited based on the expected likelihood of switching from any state to any other state.

As for the elicitation of the local and non-local priors, local prior hyperparameter c_0^{NB} was set such that $\frac{1}{\rho^j} \in (0.25, 4)$ with probability 0.95, expressing high prior probability that the HSMM is not over or under dispersed by a factor of more than 4, and non-local hyperparameters v^j , $j = 1, \dots, K$ in (2.6) are set such that the non-local prior density for ρ^j is such that $P(\rho^j \in (L_{\rho^j}, U_{\rho^j})) < 0.01$ where

$$\begin{aligned} L_{\rho^j} &:= \left\{ \rho \in (0, 1) : \text{TVD}(g^{Geom}(\cdot; \hat{\pi}_{jj}), g^{NB}(\cdot; \frac{\hat{\pi}_{jj}}{1 - \hat{\pi}_{jj}}, \rho)) = 0.1 \right\} \\ U_{\rho^j} &:= \left\{ \rho \in (1, \infty) : \text{TVD}(g^{Geom}(\cdot; \hat{\pi}_{jj}), g^{NB}(\cdot; \frac{\hat{\pi}_{jj}}{1 - \hat{\pi}_{jj}}, \rho)) = 0.1 \right\}, \end{aligned}$$

$\hat{\pi}_{jj}$ is the posterior mean of the probability of self transition for state j estimated under the HMM model, $m^j = \frac{\hat{\pi}_{jj}^j}{1 - \hat{\pi}_{jj}^j}$ is the parameter of the negative binomial distribution that recovers the geometric distribution when $\rho = 1$ and $\text{TVD}(f, g) = \frac{1}{2} \sum_{d=1}^{\infty} |f(d) - g(d)|$ is the total variation distance between discrete distributions f and g . For each state j , negligible prior density (< 0.01), is placed on regions of ρ^j whose corresponding negative binomial dwell distribution is less than 0.1 in TVD from the posterior mean estimated geometric dwell distribution. This ensures that under the HSMM, the estimated dwell distribution is forced a priori to be non-negligibly different to the HMM with very high probability.

Finally, to complete the l_1 -ball prior specification, we must elicit values for prior hyperparameters σ_β^j and a_r^j . In principle, the prior on the latent β_{pil}^j 's need only be continuous. However, the double-exponential prior in Eq. (2.2) is particularly convenient as it allows us to separate the prior specification for \mathbf{B}_p^j from the prior specification on r^j . In particular, Xu and Duan (2023) show that prior specification of Eq. (2.2) and (2.3) results in the implied prior on non-zero θ_{pil}^j 's being

$$\pi(\theta_{pil}^j | \theta_{pil}^j \neq 0) = \frac{1}{2\sigma_\beta^j} \exp\left(-\frac{|\theta_{pil}^j|}{\sigma_\beta^j}\right),$$

which is the same double-exponential prior placed on the β_{pil}^j 's. Such a property allows us to consider drawing directly from the implied prior distribution for θ_{pil}^j with desired prior expected sparsity $s^j \in (0, 1)$ as

$$\theta_{pil}^j \sim s^j \times 0 + (1 - s^j) \times \text{DExp}(0, \sigma_\beta). \quad (3.1)$$

We further assume *a priori* that the VAR process of each state j is *stable* (Lütkepohl, 2005), requiring that the reverse characteristic polynomial has no roots in the complex unit circle, i.e. $\det(\mathbf{I}_D - \mathbf{\Theta}_1^j z -$

$\dots - \Theta_p^j z^p) \neq 0$, for $|z| \leq 1$, with $z \in \mathbb{C}$, where \mathbf{I}_D denotes the identity matrix. As a result, we elicit σ_β^j to the maximal value, namely the least informative prior, that maintains a 0.95 probability that the corresponding VAR coefficients Θ^j generated according to Eq. (3.1) are stable. Once σ_β^j has been elicited, we return to the view of Θ^j as a function of \mathbf{B}^j and r^j , and set a_r^j such that the prior expected sparsity of the Θ^j 's is s^j , namely that

$$\mathbb{E}_{r \sim \text{Exp}(a_r^j)} \mathbb{E}_{\beta_p^j \sim \text{DExp}(0, \sigma_\beta^j)} \left[\frac{1}{D^2 P} \sum_{p=1}^P \sum_{i=1}^D \sum_{l=1}^D \mathbb{I}(\{\theta_{pil}^j = 0\}) \right] = s^j$$

We set $s^j = 0.75$ for all j enforcing a large degree of sparsity while still allowing for active connections when supported by the data. This two step procedure can be operationalised using Monte Carlo to estimate the probability of stability and the expected sparsity, and one-dimensional grid searches for values of σ_β^j and a_r^j satisfying the above criteria. The intercepts α^j are given the same prior as the elicited one for β_{pil}^j 's.

3.3 Results

We considered the following competing models, including our proposed approach:

- (i) The VAR-HMM model, assuming geometric dwell distributions, with l_1 -ball prior for the VAR coefficients (HMM- l_1).
- (ii) The VAR-HSMM model with negative binomial dwell distribution, local prior for ρ^j and l_1 -ball prior for the VAR coefficients (HSMM- l_1).
- (iii) The VAR-HSMM model with negative binomial dwell distribution, non-local prior for ρ^j and double exponential shrinkage prior, i.e. LASSO, (Park and Casella, 2008) for the VAR coefficients (HSMM-LASSO-NLP).
- (iv) The proposed approach, namely the VAR-HSMM model with negative binomial dwell distribution, non-local prior for ρ^j and l_1 -ball prior for the VAR coefficients (HSMM- l_1 -NLP).
- (v) Following a similar approach to Allen et al. (2014), we utilize a sliding window to estimate time-varying VAR coefficient matrices via maximum likelihood, as features to be used in a k -means clustering algorithm (with k set equal to three and two for the simulation study and application, respectively); in such a way, we obtain an estimate of the hidden state sequence. Finally, state-specific VAR matrices were reestimated using the observations assigned to each distinct state. We refer to this frequentist procedure as **VARslide**.

We assumed the prior specifications detailed as above, where the prior scale of the double exponential (LASSO) shrinkage prior in HSMM-LASSO-NLP was estimated assuming zero sparsity. The HSMM models are approximated using $\mathbf{b} = (15, 15, 15)$ which a posterior diagnostic (Figure A.3, Supplementary Material) indicated was big enough to imply negligible dwell approximation. For each Bayesian model, our procedure was run for 5,000 iterations, 1,000 of which were discarded as burn-in, while for VARSLIDE, the size of the sliding window was selected in such a way to maximize model selection performances averaged over the different states.

Table 1: Simulation Study. Estimated log-marginal likelihood (log-ml), state classification accuracy (acc) of most likely state sequence, Brier Score (BS) for state estimation, mean absolute error (MAE) of the posterior mean VAR parameter estimation and Brier Score for parameter selection under the five models considered.

Method	log-ml	acc	state - BS	VAR- MAE	VAR- BS
HMM- l_1	-113.818	1.0	3.3058×10^{-4}	1.7334×10^{-2}	8.3493×10^{-2}
HSMM- l_1	-119.651	1.0	1.1448×10^{-4}	1.7369×10^{-2}	8.3745×10^{-2}
HSMM-LASSO-NLP	-215.695	1.0	1.6205×10^{-4}	2.7277×10^{-2}	6.2000×10^{-1}
HSMM- l_1 -NLP	-113.136	1.0	1.0462×10^{-4}	1.7220×10^{-2}	8.1874×10^{-2}

Table 1 presents a summary of the results for the models (i)-(iv) models estimated to the simulated data, where we report log marginal likelihood, state accuracy (with most likely state sequence estimated through the Viterbi algorithm, [Zucchini et al. 2017](#)), state Brier score ([Brier et al., 1950](#)), mean absolute error (MAE) of the VAR coefficients (averaged across P and K), and Brier score of the VAR coefficients. For the frequentist competitor model (v), VARSLIDE, we report only accuracy (0.61) and MAE (5.81×10^{-1}), as the other metrics cannot be computed. The HSMM- l_1 -NLP achieves the highest marginal likelihood. However, somewhat surprisingly the simpler yet misspecified HMM- l_1 model achieves a higher marginal likelihood than the more complex but correctly specified HSMM- l_1 . This is likely a result of considering a relatively short time series resulting in few state transitions and the relatively uninformative LP placed on all ρ^j . In terms of state estimation, the most likely state estimated by the Viterbi algorithm for each model correctly identified the generating state sequence but the estimated state probabilities under the HSMM models can be seen to capture the behaviour of the hidden states better by achieving a small Brier Score. For the VAR parameter estimates, we see that conducting variable selection with the l_1 -ball achieves a smaller posterior MAE than using a

shrinkage prior and that the estimated inclusion probabilities were excellent according to their Brier Score. VARSLIDE appears to be by far the worst, as illustrated by low accuracy and high MAE. Overall, the HSMM- l_1 -NLP is the preferred model considering all the different metrics.

We further investigate the HSMM- l_1 -NLP results. In Figure 5 (bottom) we conduct local decoding (Zucchini et al., 2017) of the hidden state at time t , that is we display the estimated time varying probabilities $p(z_t = j | \mathbf{y}, \cdot)$, which show an excellent match with the true generating sequence. Figure 6 compares the estimated inclusion probabilities (for the order 1 VAR coefficients), in each regime, to their generating values. Firstly, we see that whenever a generating parameter was non-zero, the estimated probability of inclusion for that parameter was 1 or very close to 1. Further, generally when the estimated parameter was zero, the probability of inclusion for that parameter was away from 1 and generally very small. The exception to this is State 2, where the inclusion probabilities of truly 0 parameter are estimated to be close to 1. Interestingly, this state was not particularly sparse, having only 8 in 25 zero parameters. This suggests there may be issues with the l_1 -ball’s performance when the underlying object is not truly sparse. That being said, the l_1 -ball prior still achieves more accurate posterior mean point estimates in this state than when only using a LASSO shrinkage prior.

Similar behaviour was demonstrated for the order 2 VAR coefficients in Figure A.1. Figure A.2 further demonstrates that the posterior mean estimates values of correlation matrices $\mathbf{\Omega}^j$ are accurate to their generating values and Figure A.3 plots the posterior predictive for the dwell distribution in each state under the HMM (geometric dwell) and the HSMM with NLP.

Additional simulation results in Section A.3 of the Supplementary Material investigate selecting between a HMM and HSMM under the local and non-local priors when the data was generated from the simpler HMM. These results show that while greater evidence is found in favour of the simpler model when using the non-local prior, the complexity penalisation provided by the local prior appears to be sufficient to always select the correct model in this setting.

4 Gesture Phases Classification Using Sensor Data

4.1 Background information and data processing

We consider multivariate time series data that arise from a study on human gesture phase segmentation based on sensor data. Recent developments in new sensing technologies and modern detecting devices, as well as increased progress in processing capability, have significantly widened the research horizon

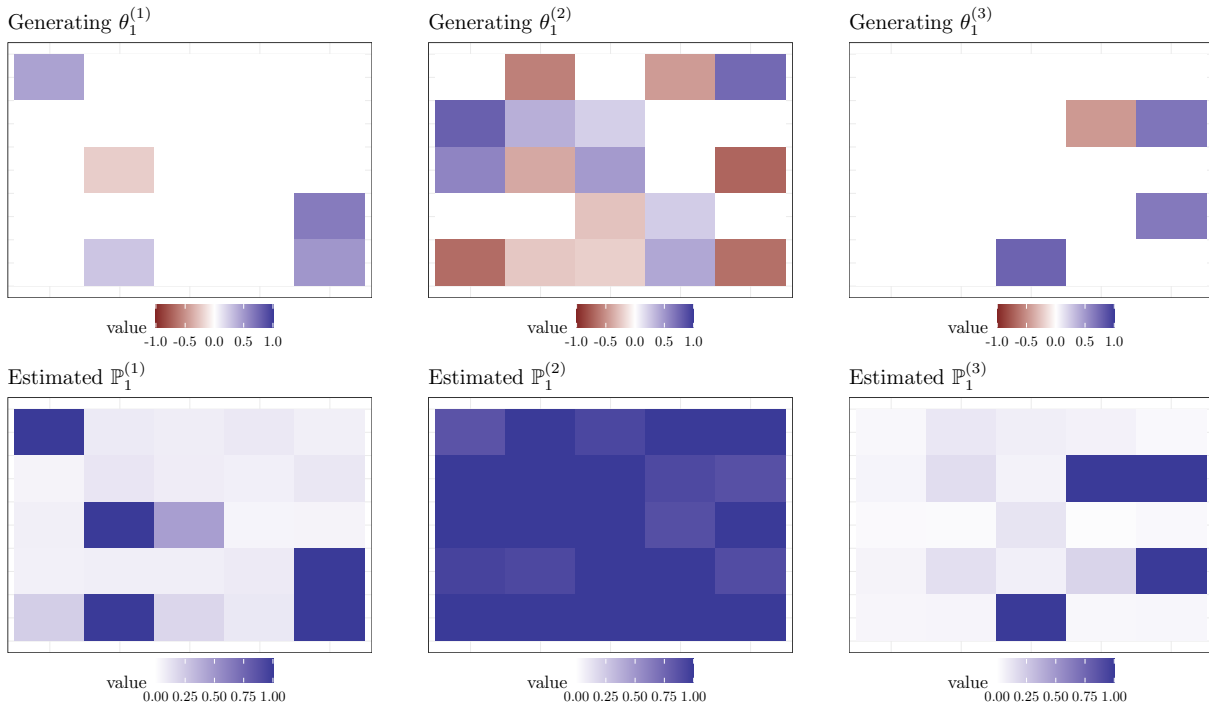


Figure 6: Simulation Study. Generating VAR parameters (order 1) and their estimated posterior probability of inclusion.

for automatic gesture analysis and human-computer interaction (Mitra and Acharya, 2007; Parvathy et al., 2021). Human gesture analysis seeks to automate tasks relevant to discourse analysis. Phase segmentation, in particular, aims at identifying and characterising the principal units, hidden states of practical relevance, and dynamical patterns involved in the gesture movement associated with these states (Moni and Ali, 2009; Wagner et al., 2014).

The dataset investigated in this article is composed by two different videos recorded using an Xbox Microsoft Kinect™ sensor, where the same user was asked to read two distinct comic strips and to tell the stories in front of the sensor (Madeo et al., 2013). As a byproduct of the Kinect™ device, scalar velocity and acceleration recordings were collected from the left hand (LF), right hand (RH), left wrist (LW), and right wrist (RW) at discrete time intervals known as frames. Measurements were obtained after normalizing the positions of the hand and the wrists according to the position of head and spine. The data were obtained from the UCI public repository <https://archive.ics.uci.edu/ml> (*Gesture Phase Segmentation DataSet*) where we used the processed version of the file provided. The same dataset was used by Madeo et al. (2013) to segment gestures from rest positions via the use of Support Vector

Machines (SVM). However, their proposed approach aimed only at segmenting the gesture streams of data, without actually characterizing the temporal dynamics relative to the different measurements and states. While we aim to model this multivariate time series dataset to identify periods of rest and active gesturing, we also intend to characterize the existence of switching and temporal dependences among acceleration and velocity measurements, whilst describing the temporal dynamics underlying these processes. Furthermore, we use our proposed approach to successfully characterise and predict a new video, corresponding to a different, unseen, story.

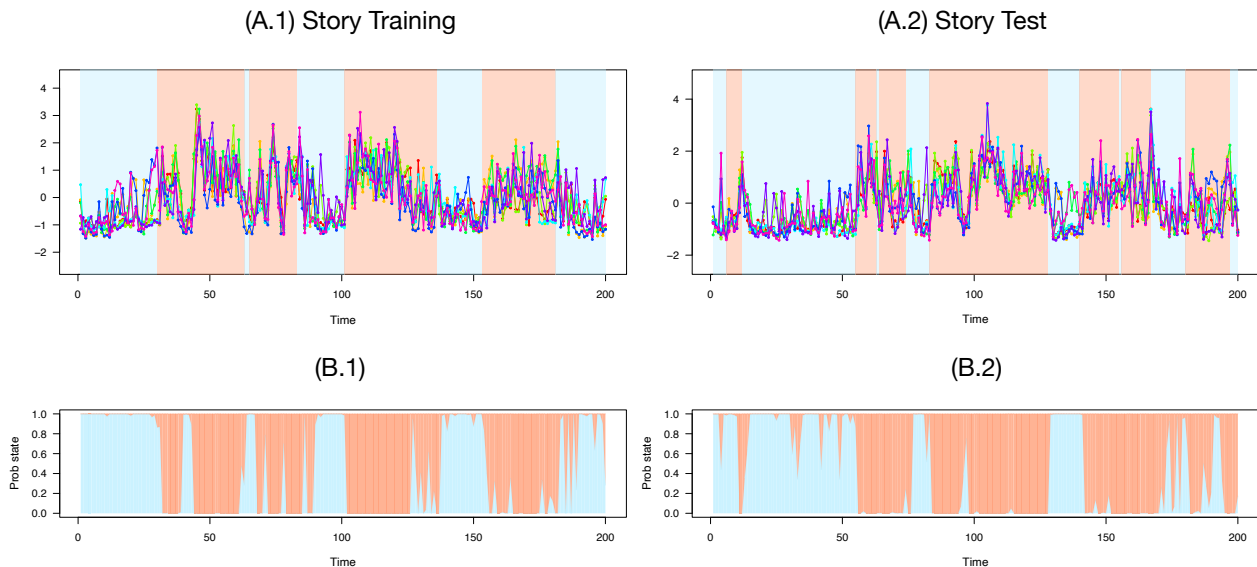


Figure 7: Gesture phase application. Training (A.1) and test (A.2) datasets. Blue vertical bands denote the true resting states, whereas red bands indicate true active states. Time varying state probabilities plots (B.1 and B.2) estimated by our proposed model, VAR-HSMM (including l_1 -ball and NLP), are also reported for both training and test stories. Our unsupervised model appears to successfully identify regime shifts between the rest position and gesture activities in a probabilistic way.

The time series we analyzed as our training dataset is shown in Figure 7 (A.1), and the story used as the test dataset is displayed in Figure 7 (A.2), where individual plots of each dimension are displayed in the Supplementary Material. They both consist of a stream of gestures resulting in $T = 200$ data points and $D = 8$ dimensions. Here, we pre-processed the original data employing the following steps: (i) smoothing, by applying a 2-point moving average filter; (ii) downsampling, by uniformly including

every 5 points (Pfenninger, 2017; Romanuke, 2021), in such a way that we are able to consider longer time lags using fewer parameters, as well as decreasing the computational complexity of our model; (iii) transforming, through the square root function (Huang et al., 2018; Hadj-Amar et al., 2023) to accommodate Gaussian emissions; (iv) standardizing, where we have scaled the time series such that each dimension $d = 1, \dots, D$ had mean 0 and variance 1. In this application we have considered the first two hundreds data points of the down-sampled dataset, for both training and test set. Gestures and rest events were manually segmented by a specialist, providing a ground truth for classification. It is clear that these physiological time series measured on different body regions during the execution of a discourse might exhibit abrupt changes in their structure as an individual experiences regime shifts between the rest position and gesture activities.

4.2 Parameter settings

We consider the different models investigated in the simulation study, considering autoregressive order $P = 1$. For the Bayesian models, we use the log-marginal likelihood (log-ml) to conduct model selection for the dwell distribution of the hidden state models and evaluate the model’s predictive accuracy for the unseen hidden states in training and on a unseen test story,for For each Bayesian model we used *stan* to sample 6,000 MCMC samples from their corresponding posterior distribution, discarding 1,000 for burn-in. The reparametrizations outlined in Section A.2 ensured that the average effective sample size of the remaining samples for all models was in excess of 1000. Figure A.6 also provides a similar diagnostic used in the Section 3.3 to demonstrate that the dwell approximation threshold \mathbf{b} was chosen large enough to well approximate the underlying HSMM.

4.3 Results

As a measure of state selection performance, we computed accuracy, sensitivity, specificity, $F1$ -score, and Matthew correlation coefficient (MCC) (see e.g. Chicco and Jurman (2020) for an excellent review about these classification measures); to evaluate prediction accuracy for the test set we report the predictive log-likelihood. Table 2 presents results for our proposed approach and Bayesian competitors, where results for the frequentist approach, (VARSLIDE) in the training set were accuracy 0.597, sensitivity 0.604, F1 0.645, and MCC 0.191, with a computational time of 8 seconds (we note that we were not able to compute those metrics for the test set since VARSLIDE does not provide an automatic framework for prediction). The estimated log-ml demonstrates that there is greater evidence in the training data

for the negative-binomial HSMM compared to the HMM and that similarly to the simulations, adopting a NLP allows for greater differentiation between the HSMM and HMM. The log-ml further supports inducing sparsity into the VAR coefficients using the l_1 -ball over shrinking the coefficients using a Bayesian LASSO type prior. With regards to the classification of the unseen ‘true’ states, the HSMM models achieve better state classification than the HMM and the NLP further improves the performance of the HSMM. While the HSMM- l_1 -NLP outperforms the HMM- l_1 in terms of state classification on the training data, their performance on the testing data is more similar. We do not, however, believe this is a result of our model over-fitting to the training set, as the model is unsupervised and never sees the class labels. The improved test set log-likelihood is a further indication that the HSMM better fits the data even though its classification point estimates are similar. While VARSLIDE is significantly faster than the other Bayesian approaches, classification performances for this data appear inferior to our proposed method and the other competitors. Section A.4 contains plots demonstrating that the HSMM-NLP model improves classification accuracy by fitting a heavier-tailed dwell distribution allowing it to estimate longer dwell times. Interestingly, we see that imposing sparsity further helps the hidden state models differentiate between states when compared with the LASSO shrinkage prior. The improved inference of the HSMM and incorporating variable selection with the l_1 -ball does come at a computational cost. Sampling from the posterior of the HSMM models is about 20 times slower than the HMM model and incorporating the l_1 -ball prior is two times slower than the shrinkage prior alternative. However we argue that the computational time is justified by the improved inference and is considerably faster than full HSMM inference (Hadj-Amar et al., 2023).

Table 2 also presents the posterior predictive performance of the models (i)-(iv) estimated on the training data to an unseen testing story. The HSMM provides an improved fit to the unseen data, particularly improving the one step ahead log predictive density, and introducing sparsity also improved predictive performance. Figure 7 (B.1, B.2) displays time varying state probabilities estimated by the HSMM-NLP model for both training and test stories, showing that our unsupervised model appears to successfully identify regime shifts between the rest position and gesture activities in a probabilistic manner. Section A.4 in Supplementary Material contains a graphical posterior predictive check consisting of the observations alongside 100 draws from the estimated posterior predictive (Gelman and Hill, 2006).

For the proposed model, Figure 8 displays the posterior probability of inclusion of the VAR coefficients (left), their estimated magnitude (center), and the correlation matrix (right), for both rest and

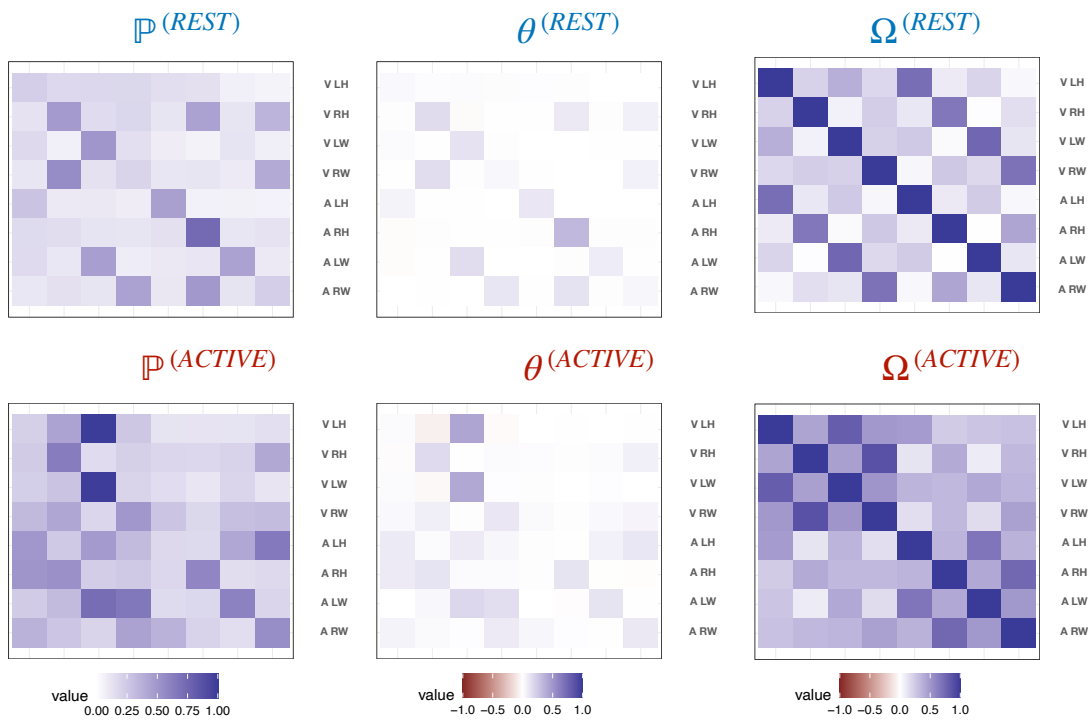


Figure 8: Gesture phase application, training story. Probability of inclusion of the VAR coefficients (left), their corresponding magnitude (center), and the correlation matrix (right), for both rest and active state.

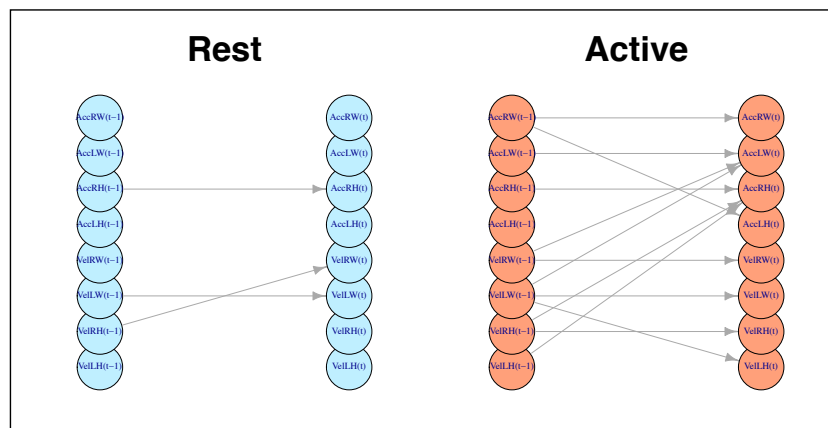


Figure 9: Gesture phase application, training story. Active edges of the VAR matrices, for both rest and active state where the directed edge is drawn if the corresponding probability of inclusion is equal or larger than 0.5.

Table 2: Accuracy, sensitivity, specificity, F1 score, Matthew correlation coefficient (MCC), and estimated log-marginal likelihood (log-ml), for both training and test dataset, for models (i)-(iv). Testing set log-ml is a one step ahead log predictive density. Run times (in seconds) of the MCMC algorithm for the training story is also reported.

		acc	sens	spec	F1	MCC	log-ml	time
Training	HMM- l_1	0.835	0.860	0.802	0.856	0.662	-1274.55	1557
	HSMM- l_1	0.850	0.877	0.814	0.870	0.693	-1272.68	34498
	HSMM-LASSO-NLP	0.760	0.903	0.570	0.811	0.511	-1280.48	14946
	HSMM- l_1 -NLP	0.890	0.903	0.872	0.903	0.776	-1266.81	24564
Test	HMM- l_1	0.860	0.920	0.784	0.880	0.716	-986.38	-
	HSMM- l_1	0.860	0.929	0.772	0.881	0.717	-980.24	-
	HSMM-LASSO-NLP	0.725	0.902	0.500	0.786	0.447	-1020.91	-
	HSMM- l_1 -NLP	0.860	0.910	0.796	0.879	0.715	-945.13	-

active states (in the training story data). The temporal nature of VAR models allows us to investigate the dynamic associations of acceleration and velocity measurements collected from LF, RH, LW, and RW. This task is carried out within each state by quantifying the probability that the associated VAR parameters are non-zero. Figure 9 shows the active edges of the VAR matrices, for both rest and active states (of the training story data) where the directed edge is drawn if the corresponding probability of inclusion is equal or larger than 0.5 (Barbieri and Berger, 2004). By investigating these plots, we can observe that the activations of the VAR parameters are different when the individual is actively telling a story and when they are resting. The magnitudes of the VAR parameters for the resting state appear to be negligible for many entries, as illustrated by the sparsity of the corresponding matrix of probabilities of inclusion; indeed, there are only three edges detected in the corresponding VAR matrix. Several interesting features can be observed from the matrix of VAR parameters for the active state: the coefficients relative to the velocities and accelerations, except for LH, are estimated as non-zero (diagonal elements of probabilities of inclusion and VAR matrices), revealing that accelerations and velocities at time $t - 1$ are relevant in characterizing the stream of gestures at time t . Furthermore, there are only two nodes with more than one (off-diagonal) edge: for the wrists, acceleration of LW is influenced by the acceleration of RW and LW at time $t - 1$; the velocities of RH and LH at time

$t - 1$ affect the acceleration of RH at time t . It is also noteworthy that the velocity of the RW at time $t - 1$ has an edge with a negative magnitude with the velocity of LH at time t , suggesting that if, for example, the velocity of RW is high, this will contribute to decreasing the velocity of LH.

While the VAR coefficients capture temporal dependencies, the correlation matrices depict contemporaneous dependencies conditional on the previous time points. The posterior mean estimates for these also show some interesting structure. In the resting state the acceleration and velocity for each location are strongly positively dependent while in the active state there is some block diagonal structure with the blocks corresponding to velocity and acceleration. In particular, greater dependence is estimated between the hand and the wrist on each side. Such findings justify our decision to estimate the full covariance matrix rather than adopt the pseudo likelihood approach of only estimating a diagonal covariance matrix often considered for VAR models (Ghosh et al., 2021). We further illustrate the time-varying behaviour among pairs of measurements (i.e. velocity LH and RH; velocity LH and LW; acceleration LH and RH; acceleration LH and LW) through posterior predictive quantiles of their corresponding time-varying correlations, as shown in Figure 10. These quantities are obtained by first drawing a state sequence and then conditioned on the drawn sequence, the time-varying sample of the parameter is stored for each MCMC iteration, so that posterior quantiles can be constructed. The correlations between velocities, and accelerations, of LH and LW (Figure 10, top and bottom left) seem to alternate between being slightly correlated for the resting states and being significantly correlated in the active states. Differently, correlations between velocities, and accelerations, of LH and RH (Figure 10, top and bottom right) appear to alternate between being slightly positive correlated and mildly correlated, showing that the contemporaneous relationship between left and right hand is not highly marked high, even during gesture activity.

5 Summary and Discussion

In this paper we have proposed a novel vector autoregressive (VAR) hidden semi-Markov model (HSMM) that allows for the modeling of complex dependencies between multivariate time series while enabling the formulation of hidden states associated with different VAR structures. The explicit-duration semi-Markovian dynamics are represented using a special structure of the transition probability matrix that can approximate the underlying HSMM with arbitrary accuracy. We have modeled contemporaneous dependencies by estimating a full covariance matrix. Furthermore, we have deployed the recently

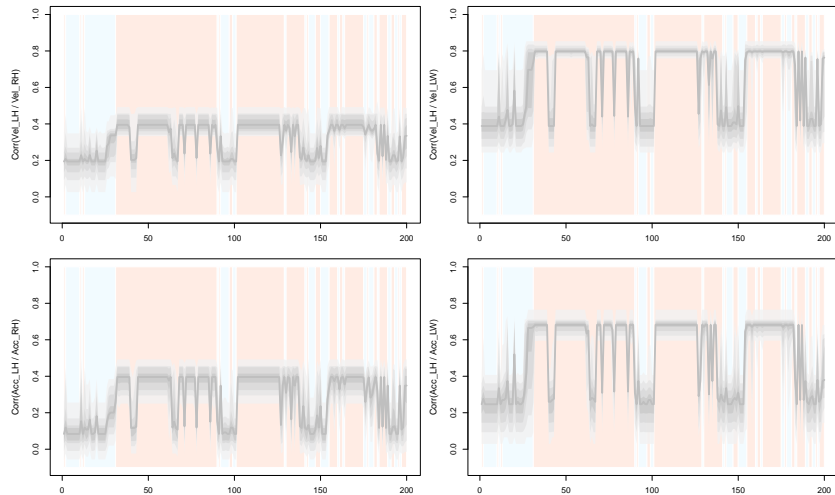


Figure 10: Gesture phase application, training story. Posterior predictive time-varying correlation among pairs of measurements, velocity LH and RH, velocity LH and LW, acceleration LH and RH, acceleration LH and LW. Blue and red vertical bands denote the estimated resting and active states, respectively.

proposed l_1 -ball prior to impose sparsity on the state-specific VAR coefficients and have used a non-local prior construction to conduct selection between the more flexible HSMM model and the simpler HMM. Our simulation results show that our model can well distinguish between different VAR regimes and that the l_1 -ball prior provides a powerful and convenient means to characterise sparse structures.

We have illustrated our proposed methodology in an application to human gesture phase segmentation based on sensor data. Overall, our approach successfully identified periods of rest and active gesturing in a probabilistic way, while also characterizing the existence of switching and temporal dependencies among acceleration and velocity measurements. We have further showed that our approach is capable of successfully characterizing and performing predictions for a new video, corresponding to a different, unseen, story.

Future work may extend our proposed approach in the following directions. First, the negative-binomial dwell distribution used in this work only allows for the modelling of overdispersed durations (i.e. variance larger than the mean), but there may be scenarios when the state durations show underdispersion. A more flexible family of dwell distribution could be provided by the COM-Poisson (Conway and Maxwell, 1962; Benson and Friel, 2021) distribution, which can account for underdispersed, overdispersed, and equidispersed dwell durations, or the discrete Weibull distribution which

“parsimoniously” captures over an under dispersion (Vinciotti et al., 2022). However, we note that increased flexibility comes with challenges, since the COM-Poisson prior has an intractable normalizing constant that increases the computational burden. Furthermore, the discrete Weibull only has its first moment in closed form complicating prior elicitation and interpretation. Second, it could be of interest to further assume a different degree of sparsity for distinct lags (in addition to different states) since the magnitude of the VAR coefficients may decrease as the lag increases. Finally, our proposed approach does not currently allow for the sparsity of the state-specific covariance matrices. The l_1 -ball projection prior may be extended to model state-specific precisions, noting that the sparsity of a precision matrix characterizes the conditional independence among variables.

Acknowledgements

The authors would like to thank David Rossell and Leo Duan for discussions about the l_1 -ball. B.H-A. and M.V. were supported by NIH-NIMH (R01-MH124115), J.J. was funded by Juan de la Cierva Formación fellowship FJC2020-046348-I.

References

- Ahelegbey, D. F., Billio, M. and Casarin, R. (2016), ‘Bayesian graphical models for structural vector autoregressive processes’, *Journal of Applied Econometrics* **31**(2), 357–386.
- Allen, E. A., Damaraju, E., Plis, S. M., Erhardt, E. B., Eichele, T. and Calhoun, V. D. (2014), ‘Tracking whole-brain connectivity dynamics in the resting state’, *Cerebral Cortex* **24**(3), 663–676.
- Barbieri, M. M. and Berger, J. O. (2004), ‘Optimal predictive model selection’, *The Annals of Statistics* **32**(3), 870–897.
- Benson, A. and Friel, N. (2021), ‘Bayesian inference, model selection and likelihood estimation using fast rejection sampling: the Conway-Maxwell-Poisson distribution’, *Bayesian Analysis* **16**(3), 905–931.
- Billio, M., Casarin, R. and Rossini, L. (2019), ‘Bayesian nonparametric sparse var models’, *Journal of Econometrics* **212**(1), 97–115.
- Brier, G. W. et al. (1950), ‘Verification of forecasts expressed in terms of probability’, *Monthly weather review* **78**(1), 1–3.

- Carpenter, B., Gelman, A., Hoffman, M., Lee, D., Goodrich, B., Betancourt, M., Brubaker, M. A., Guo, J., Li, P. and Riddell, A. (2016), ‘Stan: A probabilistic programming language’, *Journal of Statistical Software* **20**.
- Chiang, S., Guindani, M., Yeh, H. J., Haneef, Z., Stern, J. M. and Vannucci, M. (2017), ‘Bayesian vector autoregressive model for multi-subject effective connectivity inference using multi-modal neuroimaging data’, *Human brain mapping* **38**(3), 1311–1332.
- Chicco, D. and Jurman, G. (2020), ‘The advantages of the matthews correlation coefficient (MCC) over F1 score and accuracy in binary classification evaluation’, *BMC genomics* **21**(1), 1–13.
- Conway, R. W. and Maxwell, W. L. (1962), ‘A queuing model with state dependent service rates’, *Journal of Industrial Engineering* **12**(2), 132–136.
- Doan, T., Litterman, R. and Sims, C. (1984), ‘Forecasting and conditional projection using realistic prior distributions’, *Econometric reviews* **3**(1), 1–100.
- Duane, S., Kennedy, A. D., Pendleton, B. J. and Roweth, D. (1987), ‘Hybrid Monte Carlo’, *Physics Letters B* **195**(2), 216–222.
- Duchi, J., Shalev-Shwartz, S., Singer, Y. and Chandra, T. (2008), Efficient projections onto the l_1 -ball for learning in high dimensions, in ‘Proceedings of the 25th International Conference on Machine learning’, pp. 272–279.
- Fox, E. B., Hughes, M. C., Sudderth, E. B. and Jordan, M. I. (2014), ‘Joint modeling of multiple time series via the beta process with application to motion capture segmentation’, *The Annals of Applied Statistics* **8**(3), 1281–1313.
- Fúquene, J., Steel, M. and Rossell, D. (2019), ‘On choosing mixture components via non-local priors’, *Journal of the Royal Statistical Society: Series B (Statistical Methodology)* **81**(5), 809–837.
- Gefang, D. (2014), ‘Bayesian doubly adaptive elastic-net Lasso for VAR shrinkage’, *International Journal of Forecasting* **30**(1), 1–11.
- Gelman, A. and Hill, J. (2006), *Data analysis using regression and multilevel/hierarchical models*, Cambridge university press.
- George, E. I. and McCulloch, R. E. (1993), ‘Variable selection via gibbs sampling’, *Journal of the American Statistical Association* **88**(423), 881–889.
- Ghosh, S., Khare, K. and Michailidis, G. (2021), ‘Strong selection consistency of Bayesian vector

- autoregressive models based on a pseudo-likelihood approach’, *The Annals of Statistics* **49**(3), 1267–1299.
- Goebel, R., Roebroeck, A., Kim, D.-S. and Formisano, E. (2003), ‘Investigating directed cortical interactions in time-resolved fMRI data using vector autoregressive modeling and Granger causality mapping’, *Magnetic resonance imaging* **21**(10), 1251–1261.
- Gronau, Q., Singmann, H. and Wagenmakers, E.-J. (2020), ‘Bridgesampling: An R package for estimating normalizing constants’, *Journal of Statistical Software* **92**(10).
- Guédon, Y. (2003), ‘Estimating hidden semi-Markov chains from discrete sequences’, *Journal of Computational and Graphical Statistics* **12**(3), 604–639.
- Hadj-Amar, B., Finkenstädt, B., Fiecas, M. and Huckstepp, R. (2021), ‘Identifying the recurrence of sleep apnea using a harmonic hidden Markov model’, *The Annals of Applied Statistics* **15**(3), 1171.
- Hadj-Amar, B., Jewson, J. and Fiecas, M. (2023), ‘Bayesian approximations to hidden semi-Markov models for telemetric monitoring of physical activity’, *Bayesian Analysis* **18**(2), 547–577.
- Hamilton, J. D. (1989), ‘A new approach to the economic analysis of nonstationary time series and the business cycle’, *Econometrica: Journal of the econometric society* pp. 357–384.
- Hoffman, M. D. and Gelman, A. (2014), ‘The No-U-Turn sampler: adaptively setting path lengths in Hamiltonian Monte Carlo.’, *Journal of Machine Learning Research* **15**(1), 1593–1623.
- Huang, Q., Cohen, D., Komarzynski, S., Li, X.-M., Innominato, P., Lévi, F. and Finkenstädt, B. (2018), ‘Hidden Markov models for monitoring circadian rhythmicity in telemetric activity data’, *Journal of The Royal Society Interface* **15**(139), 20170885.
- Johnson, V. E. and Rossell, D. (2012), ‘Bayesian model selection in high-dimensional settings’, *Journal of the American Statistical Association* **107**(498), 649–660.
- Kadiyala, K. R. and Karlsson, S. (1997), ‘Numerical methods for estimation and inference in Bayesian VAR-models’, *Journal of Applied Econometrics* **12**(2), 99–132.
- Kalli, M. and Griffin, J. E. (2018), ‘Bayesian nonparametric vector autoregressive models’, *Journal of econometrics* **203**(2), 267–282.
- Kammerdiner, A. R. and Pardalos, P. M. (2010), Analysis of multichannel EEG recordings based on generalized phase synchronization and cointegrated VAR, *in* ‘Computational Neuroscience’, Springer, pp. 317–339.

- Langrock, R. and Zucchini, W. (2011), ‘Hidden Markov models with arbitrary state dwell-time distributions’, *Computational Statistics & Data Analysis* **55**(1), 715–724.
- Leroux, B. G. and Puterman, M. L. (1992), ‘Maximum-penalized-likelihood estimation for independent and Markov-dependent mixture models’, *Biometrics* pp. 545–558.
- Lewandowski, D., Kurowicka, D. and Joe, H. (2009), ‘Generating random correlation matrices based on vines and extended onion method’, *Journal of multivariate analysis* **100**(9), 1989–2001.
- Lütkepohl, H. (2005), *New introduction to multiple time series analysis*, Springer Science & Business Media.
- Madeo, R. C., Lima, C. A. and Peres, S. M. (2013), Gesture unit segmentation using support vector machines: segmenting gestures from rest positions, in ‘Proceedings of the 28th Annual ACM Symposium on Applied Computing’, pp. 46–52.
- Meng, X.-L. and Schilling, S. (2002), ‘Warp bridge sampling’, *Journal of Computational and Graphical Statistics* **11**(3), 552–586.
- Meng, X.-L. and Wong, W. H. (1996), ‘Simulating ratios of normalizing constants via a simple identity: a theoretical exploration’, *Statistica Sinica* pp. 831–860.
- Mitra, S. and Acharya, T. (2007), ‘Gesture recognition: A survey’, *IEEE Transactions on Systems, Man, and Cybernetics, Part C (Applications and Reviews)* **37**(3), 311–324.
- Moni, M. and Ali, A. S. (2009), HMM based hand gesture recognition: A review on techniques and approaches, in ‘2009 2nd IEEE International Conference on Computer Science and Information Technology’, IEEE, pp. 433–437.
- Ombao, H., Fiecas, M., Ting, C.-M. and Low, Y. F. (2018), ‘Statistical models for brain signals with properties that evolve across trials’, *NeuroImage* **180**, 609–618.
- Paci, L. and Consonni, G. (2020), ‘Structural learning of contemporaneous dependencies in graphical VAR models’, *Computational Statistics & Data Analysis* **144**, 106880.
- Park, T. and Casella, G. (2008), ‘The bayesian lasso’, *Journal of the American Statistical Association* **103**(482), 681–686.
- Parvathy, P., Subramaniam, K., Prasanna Venkatesan, G., Karthikaikumar, P., Varghese, J. and Jayasankar, T. (2021), ‘Development of hand gesture recognition system using machine learning’, *Journal of Ambient Intelligence and Humanized Computing* **12**(6), 6793–6800.

- Pfenninger, S. (2017), ‘Dealing with multiple decades of hourly wind and PV time series in energy models: A comparison of methods to reduce time resolution and the planning implications of inter-annual variability’, *Applied Energy* **197**, 1–13.
- Pimentel, M. A., Santos, M. D., Springer, D. B. and Clifford, G. D. (2015), ‘Heart beat detection in multimodal physiological data using a hidden semi-Markov model and signal quality indices’, *Physiological Measurement* **36**(8), 1717.
- Prado, R., Molina, F. and Huerta, G. (2006), ‘Multivariate time series modeling and classification via hierarchical VAR mixtures’, *Computational Statistics & Data Analysis* **51**(3), 1445–1462.
- Romanuke, V. (2021), ‘Time series smoothing improving forecasting’, *Applied Computer Systems* **26**(1), 60–70.
- Rossell, D. and Telesca, D. (2017), ‘Nonlocal priors for high-dimensional estimation’, *Journal of the American Statistical Association* **112**(517), 254–265.
- Samdin, S. B., Ting, C.-M., Ombao, H. and Salleh, S.-H. (2016), ‘A unified estimation framework for state-related changes in effective brain connectivity’, *IEEE Transactions on Biomedical Engineering* **64**(4), 844–858.
- Sarkar, A., Hossain, S. S. and Sarkar, R. (2023), ‘Human activity recognition from sensor data using spatial attention-aided CNN with genetic algorithm’, *Neural Computing and Applications* **35**(7), 5165–5191.
- Sims, C. A. (1980), ‘Macroeconomics and reality’, *Econometrica: journal of the Econometric Society* pp. 1–48.
- Stan Development Team (2018), ‘Stan user’s guide’.
URL: <https://mc-stan.org/docs/stan-users-guide/index.html>
- Vinciotti, V., Behrouzi, P. and Mohammadi, R. (2022), ‘Bayesian structural learning of microbiota systems from count metagenomic data’, *arXiv preprint arXiv:2203.10118* .
- Wagner, P. K., Peres, S. M., Madeo, R. C. B., de Moraes Lima, C. A. and de Almeida Freitas, F. (2014), Gesture unit segmentation using spatial-temporal information and machine learning, in ‘The Twenty-Seventh International Flairs Conference’.
- Watson, M. W. (1994), ‘Vector autoregressions and cointegration’, *Handbook of econometrics* **4**, 2843–2915.

- Xu, M. and Duan, L. L. (2023), ‘Bayesian inference with the l1-ball prior: solving combinatorial problems with exact zeros’, *Journal of the Royal Statistical Society Series B: Statistical Methodology* .
- Zen, H., Tokuda, K., Masuko, T., Kobayasih, T. and Kitamura, T. (2007), ‘A hidden semi-Markov model-based speech synthesis system’, *IEICE transactions on Information and Systems* **90**(5), 825–834.
- Zucchini, W., MacDonald, I. L. and Langrock, R. (2017), *Hidden Markov models for time series: an introduction using R*, CRC press.

A Supplementary Material

We provide supplementary material to the manuscript. Section A.1 includes the formulation of the special state transition matrix utilized to approximate the HSMM, as well as an illustrative example of such a construction. In Section A.2 we provide the details for the l_1 -ball projection algorithm. Section A.3 contains additional results of the simulation studies, and we illustrate further results of the gesture phase application in Section A.4.

A.1 State Transition Matrix

The matrix \mathbf{A} , introduced in Section 2.3, has the following structure

$$\mathbf{A} = \begin{bmatrix} \mathbf{A}_{11} & \dots & \mathbf{A}_{1K} \\ \vdots & \ddots & \vdots \\ \mathbf{A}_{K1} & \dots & \mathbf{A}_{KK} \end{bmatrix}, \quad (\text{A.1})$$

$$\mathbf{A}_{jj} = \begin{bmatrix} 0 & 1 - \phi_j(1) & 0 & \dots & 0 \\ \vdots & 0 & \ddots & & \vdots \\ & \vdots & & & 0 \\ 0 & 0 & \dots & 0 & 1 - \phi_j(b_j - 1) \\ 0 & 0 & \dots & 0 & 1 - \phi_j(b_j) \end{bmatrix}, \quad \mathbf{A}_{jk} = \begin{bmatrix} \pi_{jk} \phi_j(1) & 0 & \dots & 0 \\ \pi_{jk} \phi_j(2) & 0 & \dots & 0 \\ \vdots & & & \\ \pi_{jk} \phi_j(b_j) & 0 & \dots & 0 \end{bmatrix}, \quad (\text{A.2})$$

where the sub-matrices \mathbf{A}_{jj} along the main diagonal, of dimension $b_j \times b_j$, are defined for $b_j \geq 2$, and $\mathbf{A}_{jj} = 1 - \phi_j(1)$, for $b_j = 1$. The $b_j \times b_k$ off-diagonal matrices \mathbf{A}_{jk} are 0 except for the first column which contains *hazard rates* defined for $r \in \mathbb{N}_{>0}$

$$\phi_j(r) = \frac{p(d_j = r | \boldsymbol{\lambda}_j)}{p(d_j \geq r | \boldsymbol{\lambda}_j)}, \quad \text{if } p(d_j \geq r - 1 | \boldsymbol{\lambda}_j) < 1, \quad (\text{A.3})$$

and 1 otherwise, where $p(d_j = r | \boldsymbol{\lambda}_j)$ denotes the probability mass function of the dwell distribution $g(\boldsymbol{\lambda}_j)$ for state j . This structure for the matrix \mathbf{A} implies that transitions within state aggregate B_j are determined by diagonal matrices \mathbf{A}_{jj} , while transitions between state aggregates B_j and B_k are controlled by off-diagonal matrices \mathbf{A}_{jk} .

A.2 l_1 -Ball Projection Algorithm

The algorithm of Xu and Duan (2023) to compute the l_1 -ball projection solving (2.3) is provided in Algorithm A.1

Algorithm A.1 l_1 -ball projection. **Input:** $\beta_p^j \in \mathbb{R}^{D^2}$ and $r^j \in \mathbb{R}_+$. **Output:** $\Theta_p^j \in \mathbb{R}^{D \times D} \cup \{0\}$

if $\|\beta_p^j\|_1 \leq r^j$ **then**

$$\Theta_p^j \leftarrow \text{vec}^{-1}(\beta_p^j)$$

else

Sort β_p^j so that $|\beta_{p(1)}^j| \geq \dots \geq |\beta_{p(D^2)}^j|$

$$\phi_l \leftarrow \left(\sum_{n=1}^l |\beta_{p(n)}^j| - r^j \right)_+, \quad \text{for } l = 1, \dots, D^2.$$

$$m \leftarrow \max \left\{ n : |\beta_{p(n)}^j| > \frac{\phi_n}{n} \right\}$$

$$\tilde{\phi} \leftarrow \frac{\phi_m}{m}$$

$$\theta_{pi}^j \leftarrow \text{sign}(\beta_{pi}^j) \max \left(|\beta_{pi}^j| - \tilde{\phi}, 0 \right), \quad \text{for } l = 1, \dots, D^2.$$

$$\Theta_p^j \leftarrow \text{vec}^{-1}(\theta_p^j)$$

end if

While *stan* and NUTS attempt to adapt sampling to the geometry of the posterior, reparametrizations of the sample space can help to facilitate this in high dimensions: i) we reparametrized the latent variables for the VAR coefficients as $\tilde{\beta}^j := \frac{\beta^j}{\sqrt{T}}$ motivated by the fact that as the sample size grows the posterior of the β^j does not concentrate; ii) we reparameterized the l_1 -ball radius as $\tilde{r}^j := \frac{r^j}{\sqrt{D^2 P}}$ motivated by the fact that the radius is learned from the $D^2 P$ elements of θ^j ; iii) we found that reparametrizing dwell parameters $\tilde{p}^j := \frac{\lambda^j}{1+\lambda^j}$ and $\tilde{q}^j := \frac{\rho^j}{1+\rho^j}$ for the HSMM, more closely resembling the parameterization of the HMM, also improved performance. The above reparametrizations facilitate posterior sampling while leaving the model unchanged.

A.3 Additional Simulation Results

For the simulated data as described in Section 3.3, Figure A.1 compares the estimated inclusion probabilities of the order 2 VAR coefficients in each regime, Θ_2^j , to their generating values. Similarly to the order 1 estimates, all non-zero generating parameters are estimated to have close to 1 probability of inclusion and most truly 0 estimates have a small probability of inclusion. The exception is still State 2 where the generating VAR estimates were not particularly sparse.

Figure A.2 compares the posterior mean estimates for Ω^j with the data generating values. As the data was standardised, we compare estimated and generated values for pairwise correlations Ω^j rather than covariances Σ^j . For States 2 and 3 the posterior mean estimate for correlation matrix Ω^j very closely resemble the generating values while the estimates for State 1 are reasonable.

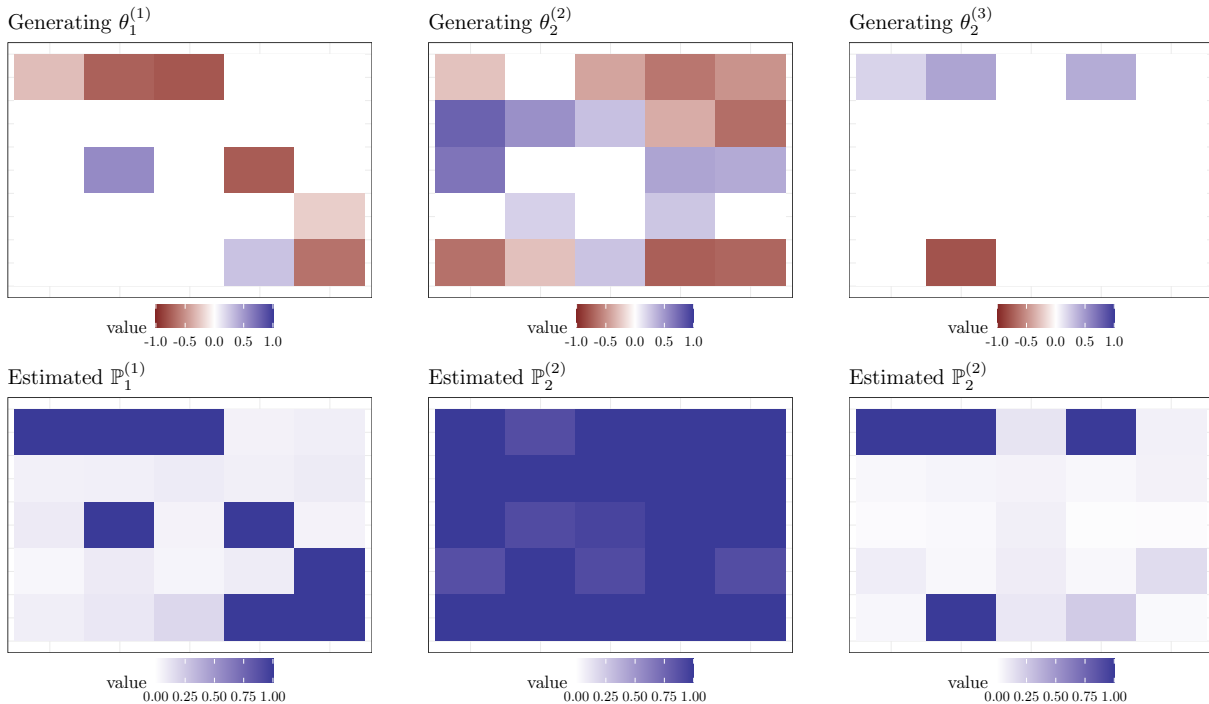


Figure A.1: Simulation Study. Generating VAR parameters (order 2) and their estimated posterior probability of inclusion.

Finally, Figure A.3 plots the posterior predictive distributions for the dwell distribution in each state estimated under the HMM (geometric dwell) and the negative binomial HSMM. For the HSMM we plot both the posterior predictive for our model’s approximation to the HSMM dwell and the exact negative binomial dwell that would correspond to the same parameters. Such a plot demonstrates that taking $\mathbf{b} = (15, 15, 15)$ was sufficiently large to provide negligible approximation of the fitted dwell distribution.

For completeness, we conducted a further simulation exercise, this time simulating a $D = 5$ dimensional time series of $T = 200$ from a $K = 2$ state HMM with VAR emission distribution of order $P = 1$ in each regime. The self transition probabilities in each state were set to $\tilde{\pi}_{jj} = 0.9$ for $j = 1, 2$. The VAR parameters, intercepts and covariance in each regime were generated according to the procedure outlined as in the previous simulation, where the VAR had 70% sparsity in State 1 and 30% sparsity in State 2. We repeated the simulation of the time series 10 times. For each simulation we considered selecting between the generating HMM model and the more complex HSMM models under the local and non-local priors.

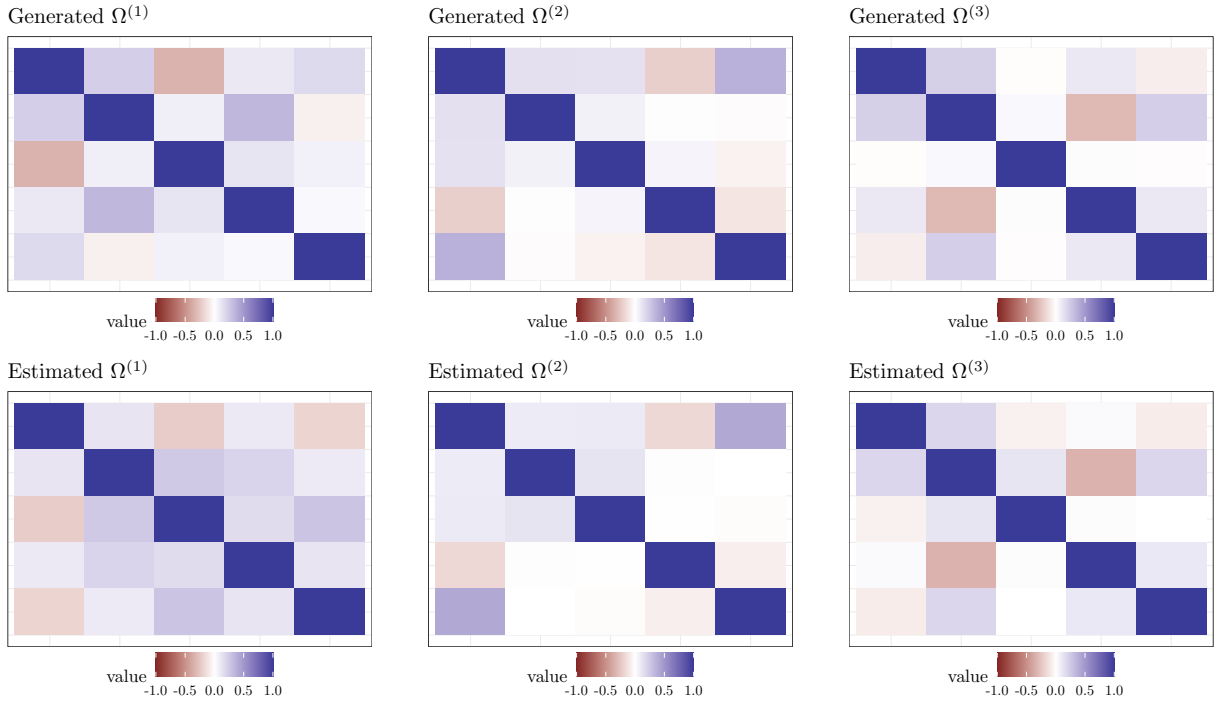


Figure A.2: Simulation Study. Generating correlation matrices and their estimated posterior means.

Figure A.4 compares the difference in log-ml of the HMM- l_1 model with that of the HSMM- l_1 and HSMM- l_1 -NLP models across the 10 repeats. Under the NLP the difference in log-ml between the HMM and HSMM is more positive, indicating that the model selection decision correctly favours the simpler HMM model to a greater extent. However, under the LP this difference is also always positive indicating that the correct model selection decision is still made here. This is particularly reassuring as the number of state transitions in a time series is often many fewer than the number of observations and so HMM/HSMM dwell distribution are often estimated using few data points.

A.4 Additional Gesture Phase Segmentation Results

For the gesture phase segmentation application described in Section 4, Figure A.5 plots the individual dimensions of the training and testing data, shown jointly in Figure 7, along side 100 draws from the estimates posterior predictive and the MAP state classification.

Figure A.6 is analogous to Figure A.3 and plots the posterior predictive distributions for the dwell distribution in each state estimated under the HMM (geometric dwell) and the exact and approximate negative binomial HSMM. This demonstrates that taking $\mathbf{b} = (15, 15, 15)$ was sufficiently large to

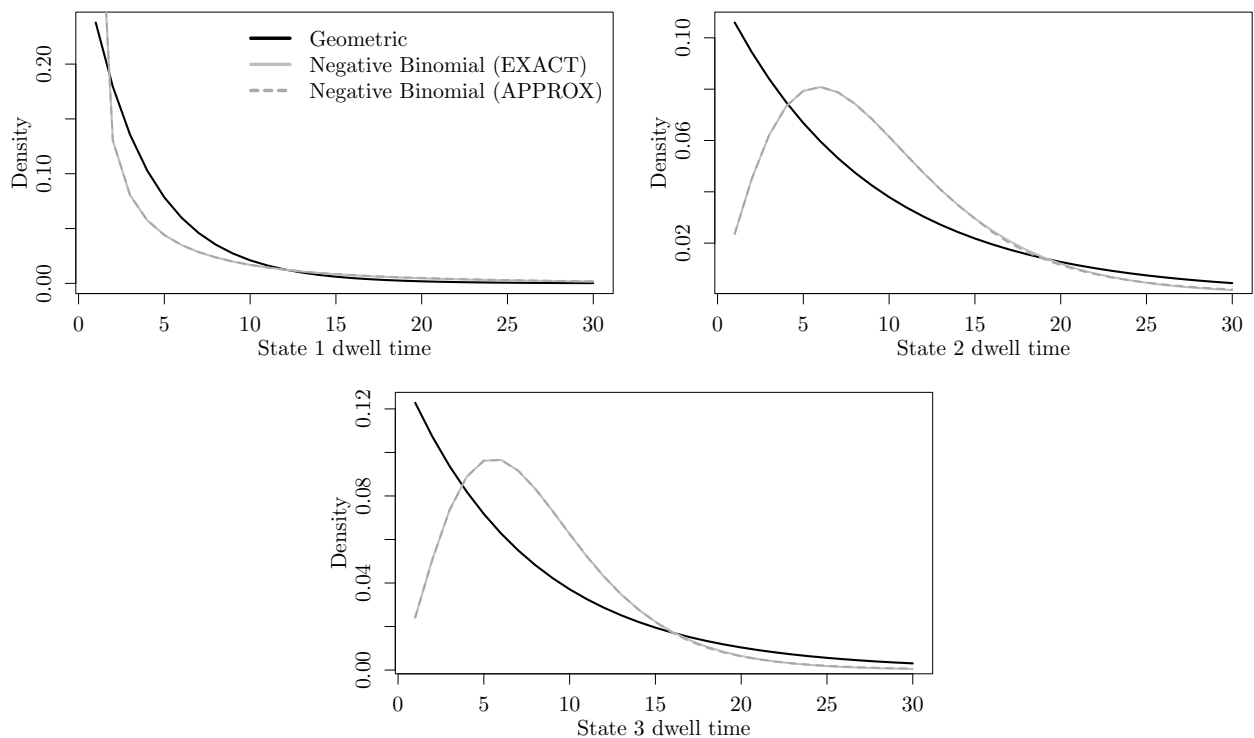


Figure A.3: Simulation Study. Posterior predictive dwell distributions for each states under the HMM (geometric dwell), the approximation to the negative binomial HSMM resulting from $\mathbf{b} = (15, 15, 15)$ and the exact negative binomial HSMM dwell distribution corresponding to the same parameter posterior.

provide negligible approximation of the fitted dwell distribution.

We plotted the estimated dwell distributions under the HMM, HSMM and HSMM-NLP and compared these with the empirical dwell distributions provided by the supervised states for both the training and testing data in Figure A.7. We see here that the HSMM-NLP is able to fit a heavier tailed dwell distribution (corresponding to $\rho < 1$) and is able to assign higher mass to the longer dwell times associated with the supervised states.

Remembering, that our model treats the states as unlabelled, Figures A.8 and A.9 further plots the estimated dwell distribution under the HMM, HSMM and HSMM-NLP and compared this to the empirical distributions of the dwells times in their MAP estimated state sequence for the training and testing sets respectively. We see that the increased mass on longer dwells observed in Figure A.7 allows the HSMM-NLP to estimate longer dwell times than the other methods and achieve better

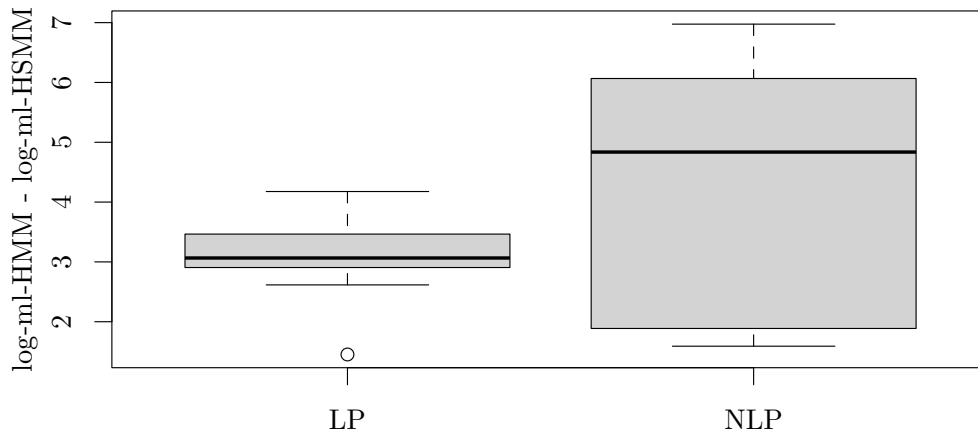


Figure A.4: Simulation Study. Comparison of $HMM-l_1$ log-ml with $HSMM-l_1$ and $HSMM-l_1$ -NLP across 10 repeat datasets drawn from the simpler HMM model. Positive values indicate correctly selecting the simpler HMM model.

correspondence with the supervised state assessment.

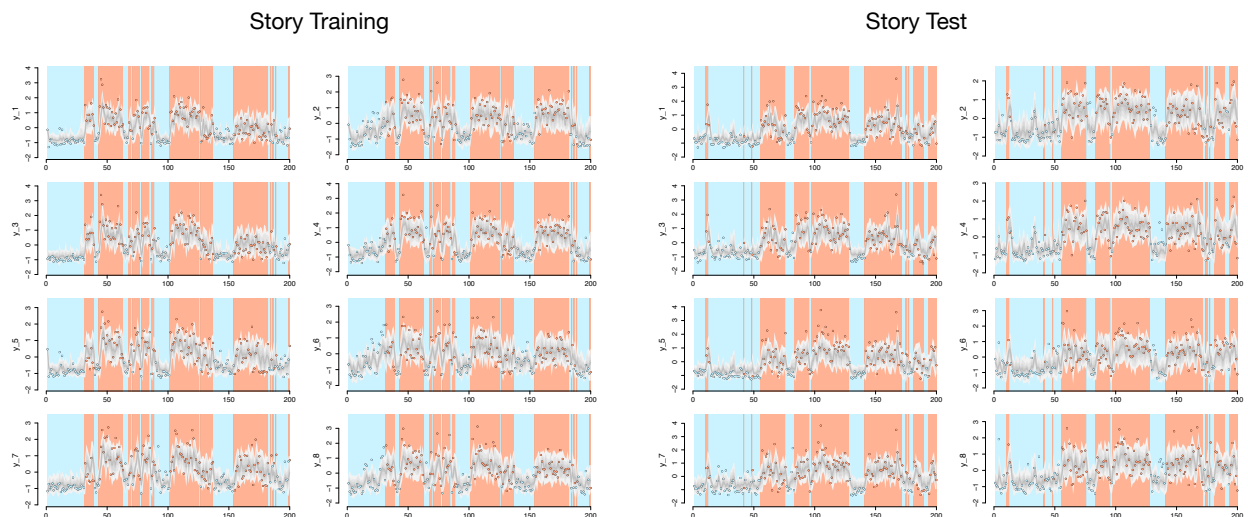


Figure A.5: Gesture phase application. Graphical posterior predictive check consisting of the observations alongside 100 draws from the estimated posterior predictive, for both training story (left) and test story (right).

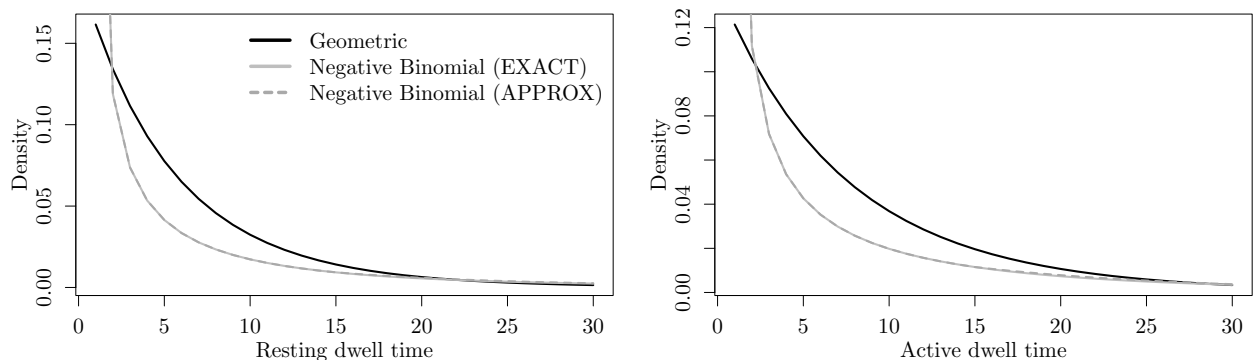


Figure A.6: Gesture phase application. Posterior predictive dwell distributions for each states under the HMM (geometric dwell), the approximation to the negative binomial HSMM resulting from $\mathbf{b} = (15, 15)$ and the exact negative binomial HSMM dwell distribution corresponding to the same parameter posterior.

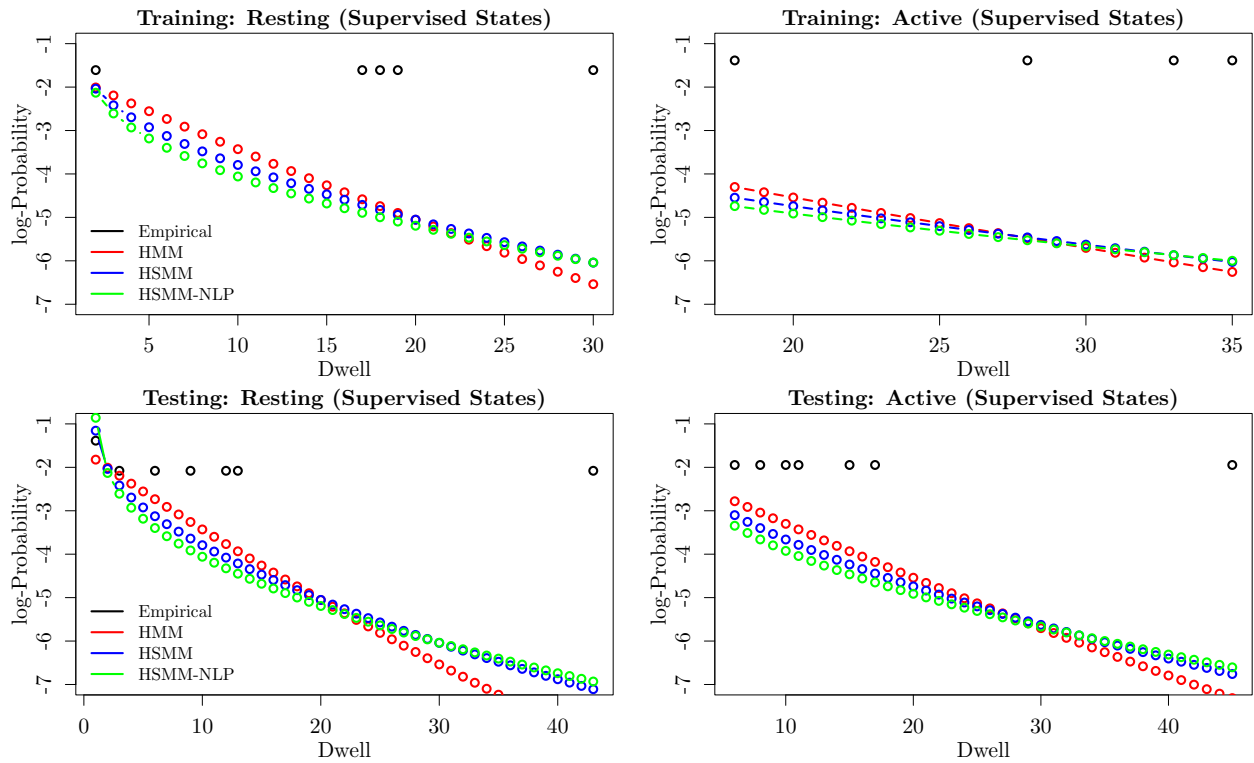


Figure A.7: Comparison of the estimated dwell distributions under the HMM, HSMM and HSMM-NLP with the empirical distribution of the supervised states in resting and active states in *training* (**top**) and *testing* (**bottom**) on the log-probability scale.

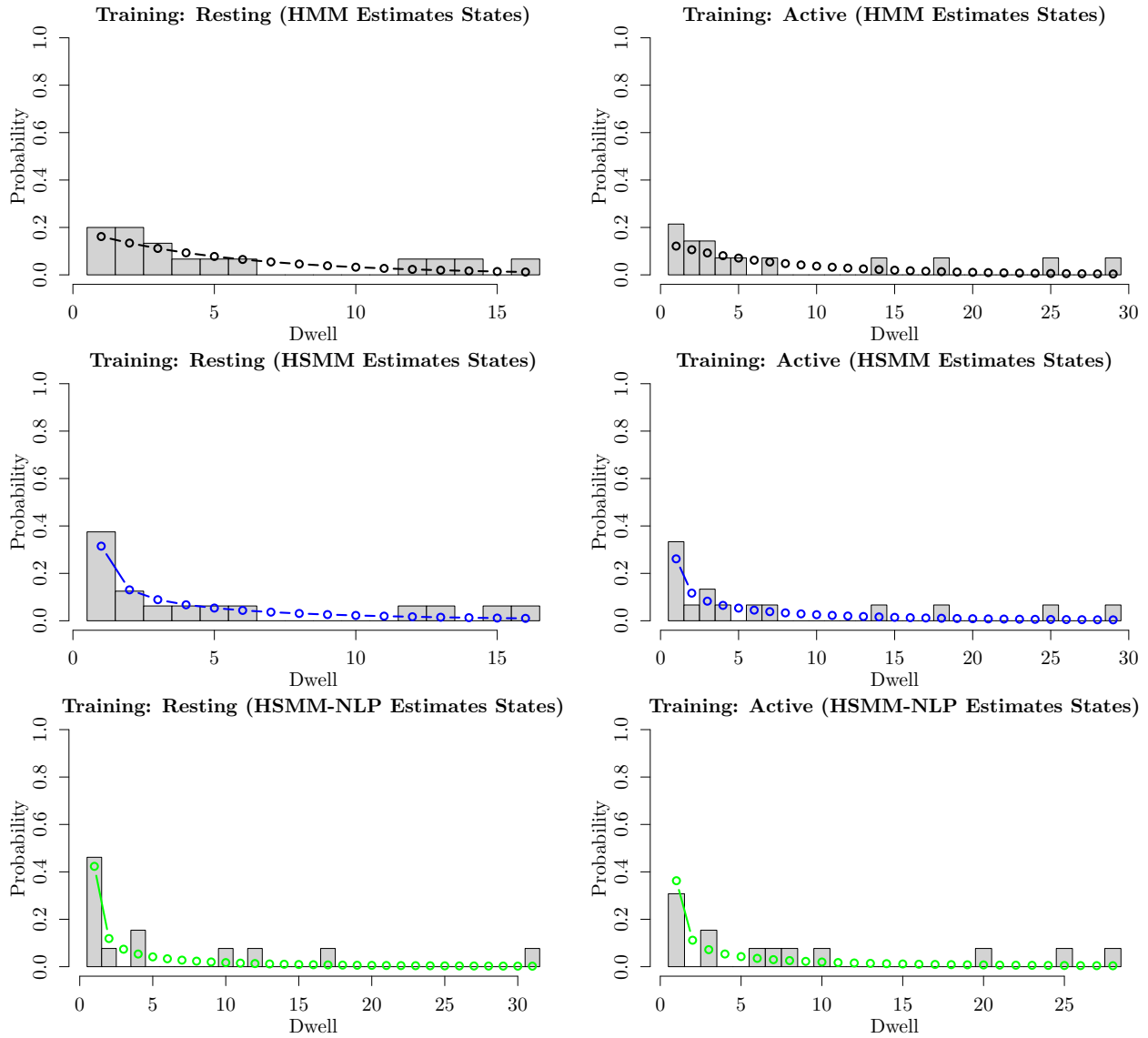


Figure A.8: Comparison of the estimated dwell distributions under the HMM, HSMM and HSMM-NLP alongside the empirical distribution of the dwell times in the MAP estimated state sequence for the *training* data.

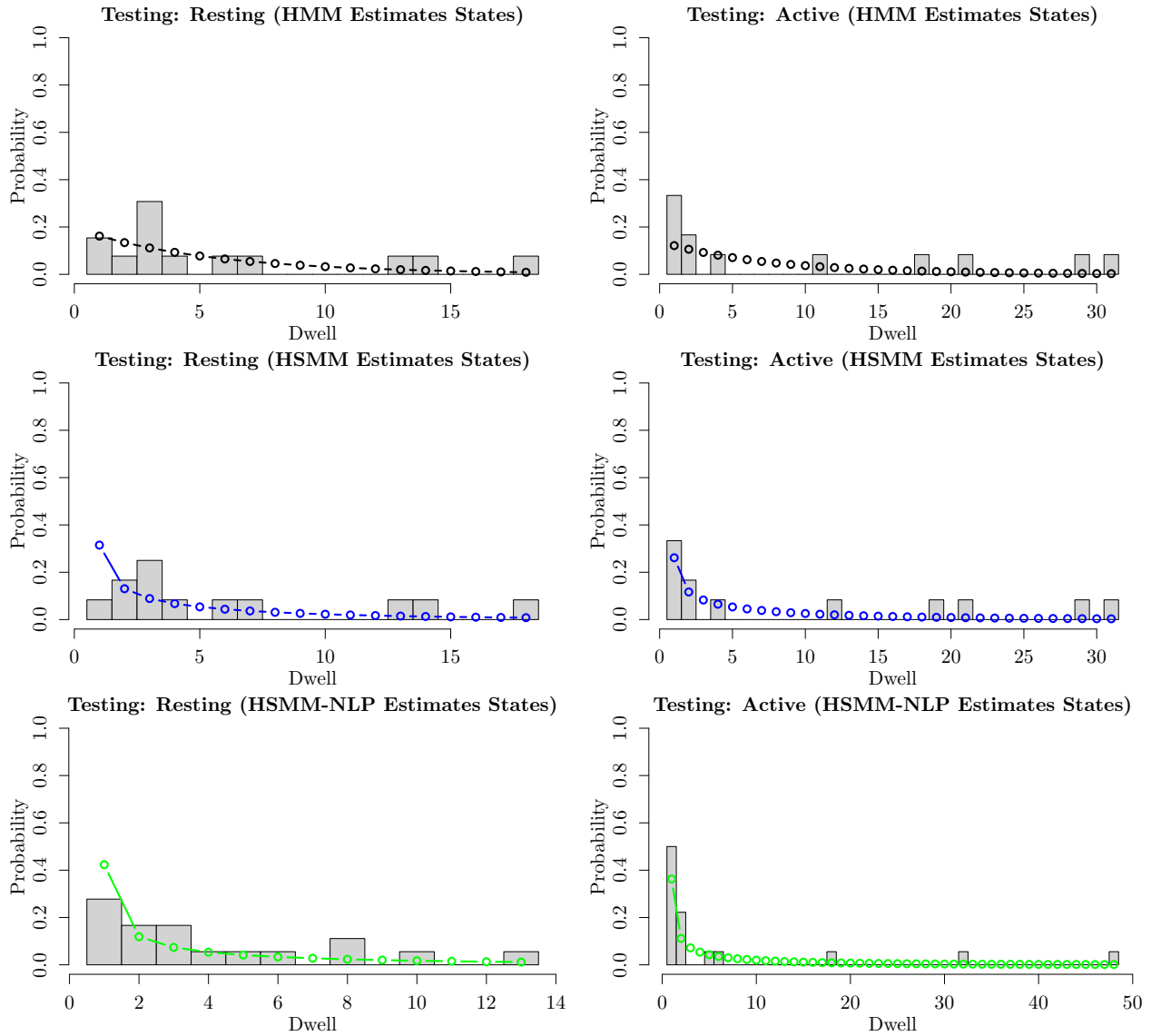


Figure A.9: Comparison of the estimated dwell distributions under the HMM, HSMM and HSMM-NLP alongside the empirical distribution of the dwell times in the MAP estimated state sequence for the *testing* data.